Sustainable Energy Technologies and Assessments 93 (2026) 105361

Contents lists available at ScienceDirect

Sustainable Energy Technologies and Assessments

journal homepage: www.elsevier.com/locate/seta

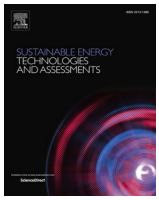

Solar hybrid sulphur cycle demonstration plant (Part A): Techno-economic assessment of solar thermal plant from the European Union-HySelect project

Y. Kadohiro [a,*], J.H.S. Martins [a], D. Dimitrakis [a], D. Thomey [a], N. Monnerie [a], C. Sattler [a,b], J. Michels [c], M. Kürten [c], M. Lanchi [d], R. Liberatore [d], L. Turchetti [d]

[a] Deutsches Zentrum für Luft- und Raumfahrt, Institute of Future Fuels, Linder Höhe, 51147 Cologne, Germany
[b] RWTH Aachen University, Chair for Solar Fuel Production, Aachen, Germany
[c] Grillo Chemicals GmbH, Buschstraße 95, 47166 Duisburg, Germany
[d] ENEA, Italian National Agency for New Technologies, Energy and Sustainable Economic Development, Italy

ARTICLE INFO

Keywords:
Hybrid sulphur cycle
Solar thermal energy
Energy demand analysis
Cost estimation
Demonstration plant

ABSTRACT

The Hybrid Sulphur (HyS) cycle is attracting interest for decarbonising the sulphuric acid industry by integrating concentrating solar thermal (CST) technologies with the high-temperature acid splitting process. Several energy and cost studies have been performed and significant European Union (EU)-funded research projects have been implemented so far to bridge the gap towards the commercialisation of the HyS concept. However, even the concept development at the demonstration plant scale has not yet been achieved. Within the EU-HySelect project, this study presents the first demonstration-scale techno-economic assessment of the HyS plant's solar thermal and thermochemical subsystems, utilising a detailed component-level costing approach to advance the Technology Readiness Level. The specific energy of solar SO_2 production (at purity of 79.4 wt%, compressed at 1.3 MPa) and the total solar demonstration plant costs are calculated based on Aspen Plus at 15.62 MJ/kg (or 4.34 kWh/kg) and 3.4–6.1 million $€_{2025}$, respectively. Unlike idealised models that ignore industrial constraints, this study aligns with practical standards to realistically assess implementation potential. It identifies critical bottlenecks in CST technology and the sulphuric acid splitting reactor, highlighting key pathways for scale-up. The reported cost estimates further establish a concrete baseline for future HyS research and industrial decarbonisation strategies.

1. Introduction

The Hybrid Sulphur (HyS) Cycle for hydrogen (H_2) production, originally proposed by Westinghouse Electric Corporation in 1975 [1], is gaining more attention especially considering the decarbonisation potential of the sulphuric acid (H_2SO_4) industry and circularity aspects (e.g. recycling of spent H_2SO_4). It consists of four main processes: (i) H_2SO_4 dissociation and sulphur trioxide (SO_3) splitting, (ii) Sulphur dioxide (SO_2) and Oxygen (O_2) separation, (iii) SO_2-Depolarised Electrolysis (SDE), and (iv) H_2SO_4 concentration. The chemical reaction equations and associated parameters for two key processes, (i) and (iii), are detailed in Table 1 [2,3].

In process (i), H_2SO_4 first dissociates into SO_3 and water vapour at 623–673 K via a spontaneous vapour-phase equilibrium (Reaction 1). The resulting SO_3 is then catalytically decomposed to SO_2 and O_2 at 973–1273 K (Reaction 2). Conversely, process (iii) feeds SO_2 dissolved in liquid H_2SO_4 (30–70 %) to the SDE anode, where it oxidizes to H_2SO_4 (Reaction 3). Protons subsequently crossover through a polymer membrane to the cathode, combining with electrons to produce H_2 (Reaction 4).

The HyS cycle is a hybrid thermochemical water splitting process incorporating an electrochemical step. Like many cycles proposed over the past five decades [4,5], it offers a promising approach for carbon-free H_2 production. Thermochemical methods are generally preferred due to their superior scalability and efficiency relative to biological or purely electrochemical methods. Among these, sulphur-based cycles (specifically Sulphur-Iodine (S-I) and HyS) are top contenders because of their high theoretical energy efficiency (approximately 50 %) and operating temperatures below 1273 K [4,6]. The HyS cycle is

* Corresponding author.
E-mail address: Yasuki.Kadohiro@dlr.de (Y. Kadohiro).

https://doi.org/10.1016/j.seta.2026.105361
Received 7 May 2026; Received in revised form 21 August 2026; Accepted 25 August 2026

Nomenclature

Abbreviation

AWE	Alkaline Water Electrolysis
CEPCI	Chemical Engineering Plant Cost Index
COP	Coefficient of Performance
CSP	Concentrated Solar Power
CST	Concentrating Solar Thermal
DLR	German Aerospace Centre
EPA	Environmental Protection Agency
EU	European Union
HyS	Hybrid Sulphur
LCOH	Levelised Cost of Hydrogen
LHV	Lower Heating Value
OSHA	Occupational Safety and Health Administration
O&M	Operation and Maintenance
PEM	Proton Exchange Membrane
PEME	Proton Exchange Membrane Electrolysis
PTFE	Polytetrafluorethylen
PV	Photovoltaic
RMP	Risk Management Plan
S-I	Sulphur-Iodine
SDE	SO_2-Depolarised Electrolysis
SOEL	Solid Oxide Electrolysis
TEA	Techno-Economic Asessment
TES	Thermal Energy Storage
TRL	Technology Readiness Level
WHSV	Weight Hourly Space Velocity

Chemical formula

Al	Aluminum
Cl	Chlorine
Cr	Chromium
Cu	Copper
Fe	Iron
Fe_2O_3	Iron (III) oxide
H_2	Hydrogen
H_2SO_4	Sulphuric acid
O_2	Oxygen
SiC	Silicon Carbide
SiSiC	Silicon-Infiltrated Silicon Carbide
SO_2	Sulphur dioxide
SO_3	Sulphur trioxide

Latin symbols

EC	Equipment cost. €
e	Specific energy. J/kg
f^0	Liquid fugacity of pure component. MPa
ΔG_0	Standard Gibbs free energy change. kJ/mol
H	Enthalpy. kJ/mol
ΔH_0	Standard enthalpy change. kJ/mol
I	CEPCI.
$\dot{m}$	Mass flow rate. kg/s
$\dot{n}$	Molar flow rate. kmol/s
P	System pressure. MPa
$\dot{Q}$	Thermal power. W_{th}
R	Gas constant. J/(K·mol)
S	Characteristic capacity
T	Temperature. K
W	Electric power. W_{el}
x	Mole fraction in the liquid phase
y	Mole fraction in the vapour phase

Greek symbols

γ	Activity coefficient in the liquid phase
η	Efficiency
φ	Fugacity coefficient in the vapour phase

Subscripts and Superscripts

acid	Sulphuric acid
d	Equipment specific scale factor
E	Excess
helio	Heliostat
H2	Hydrogen
i	component or ionic species
m	Molecular species
PP	Power cycle efficiency (W_{el}/W_{th})
rec	Receiver
ref	Reference year
STH	Solar-to-Hydrogen

particularly attractive due to its low electrical demand and simplified two-step configuration. Specifically, the incorporation of SDE reduces the required cell voltage to −0.158 V at 298 K, substantially lower than state-of-the-art Proton Exchange Membrane (PEM) water electrolysis (−1.229 V at 298 K) [7].

When integrated with renewables, the HyS cycle produces green hydrogen suitable for replacing fossil fuels. Concentrating Solar Thermal (CST) systems are ideally suited to H_2SO_4 splitting due to their high thermal capacity (>1273 K); at these temperatures, direct electrification via solar Photovoltaic (PV) or wind is often inefficient [8]. The CST's compatibility with Thermal Energy Storage (TES) further ensures a cost-effective and dispatchable heat supply [9]. According to the classification proposed by Singh and McGregor [10], fourth-generation CST systems, with Technology Readiness Levels (TRLs) of 4–8, operating temperatures above 873 K, and concentration ratios of 500–1000+, are suitable candidates for integration with the HyS cycle. Notable examples include German Aerospace Centre (DLR)'s centrifugal particle receiver "CentRec" [11] and Synhelion's absorbing gas receiver [12], both capable of exceeding process temperatures.

Several energy demand analysis studies of the HyS cycle have already been conducted to identify the performance levels required for commercialisation of the concept. Gorensek et al. [13,14] have

Table 1
Summary of chemical reaction equations and associated parameters for two key processes: (i) H_2SO_4 dissociation and SO_3 splitting, (iii) SDE. ΔH_0 and ΔG_0 are the standard enthalpy change (kJ/mol) and the standard Gibbs free energy change (kJ/mol), respectively [2,3].

Process	Equation	Temperature range (K)	Thermodynamic quantity (kJ/mol)	Endothermic or Exothermic?
H_2SO_4 dissociation	$H_2SO_4(aq) \leftrightarrow SO_3(g) + H_2O(g)$ (1)	623–673	$\Delta H_0 = +98$	Endothermic
SO_3 splitting	$SO_3(g) \leftrightarrow SO_2(g) + \frac{1}{2}O_2(g)$ (2)	973–1273	$\Delta H_0 = +99$	Endothermic
SDE (Anode)	$SO_2(aq) + 2H_2O(l) \rightarrow H_2SO_4(aq) + 2H^+(aq) + 2e^-$ (3)	< 393	$\Delta G_0 = +30$	Exothermic
SDE (Cathode)	$2H^+(aq) + 2e^- \rightarrow H_2(g)$ (4)			

developed the HyS concept coupled with a high-temperature nuclear heat source and showed a thermochemical process efficiency (based on the H_2 Lower Heating Value – LHV) of 35–40 %. Guerra-Niehoff et al. [15] investigated the HyS concept coupling with a Concentrated Solar Power (CSP) plant, and found that the efficiency of the thermochemical process (based on the H_2 LHV) can be close to 30 %. Gorensek et al. [16] also built a HyS cycle model coupled with a falling particle concentrated solar receiver, and their model calculated a thermochemical process efficiency and solar-to-H_2 efficiency of 35 % and 17 % (based on the H_2 LHV), respectively. Batgi and Dincer [17] have developed a multigenerational integrated system that includes a HyS system, a solar tower system, a thermochemical heat pump system, and a multi-effect desalination system in order to produce fresh water and H_2 as final products. Their energy demand analysis showed that the overall energy efficiency (based on the H_2 LHV and the enthalpy difference of fresh water) was 8.15 %.

With regard to the cost analysis, Corgnale et al. [18] evaluated the Levelised Cost of H_2 (LCOH) for a commercial HyS plant, employing a falling particle concentrated solar receiver as a heat source, with an operational lifetime of 40 years, reporting the LCOH of 3.19–4.80 US $/kg. Del Fabbro Arcopinto et al. [19] investigated the LCOH for the commercial HyS plant coupled with a CST system with the operational lifetime of 20 years, reporting the LCOH of 6.72 €/kg. Zuleta Marin et al. [20] conducted a Techno-Economic Assessment (TEA) of the solar HyS plant integrated with the Chilean copper industry for the co-production of H_2 and O_2. The CST system utilizing molten salt was employed to supply heat for the H_2SO_4 dissociation process, while electric heater was utilised for the SO_3 splitting process. Their study reported the LCOH of 5.74 ± 1.04 €/kg, based on a plant lifetime of 20 years.

From an international collaboration perspective, several projects have been carried out to advance HyS technology. Table S1 in the Supplementary File provides the list and comparison of HyS cycle-related European Union (EU) projects. The earliest, EU-HYTHEC [21,22] (2004–2007), primarily demonstrated nuclear- and solar-based S-I cycle feasibility, with secondary HyS emphasis. A prototype volumetric solar receiver-reactor for direct SO_3 splitting underwent extensive numerical [23] and experimental [24] validation. Process simulation and cost analysis for HyS plants integrated with a 50 MW CST system near Lake Nasser, Egypt, estimated hydrogen production at 5.73 €/kg [25]. EU-HycycleS [26] (2008–2011) qualified materials, catalysts, and components for high-temperature H_2SO_4 splitting in nuclear- and solar-based S-I and HyS plants. The receiver-reactor was redesigned with a two-chamber configuration for solar-driven H_2SO_4 dissociation and SO_3 splitting, validated numerically [27] and experimentally [28]. Extensive catalyst screening and 100-hour stability testing showed Silicon Carbide (SiC) coated with a Chromium-Iron (Cr-Fe) mixed oxide ($Fe_{0.7}Cr_{1.3}O_3$) exhibited superior H_2SO_4 corrosion resistance with SO_3 conversion exceeding 70 % [29–31]. TEA estimated LCOH at 7.80 €/kg for solar HyS plants, though methodology details were undisclosed. EU-SOL2HY2 [32] (2013–2016) analysed the solar-integrated HyS cycle in detail. Receiver-reactor scaling was based on prior validation [33], while a modified concept with separate receiver and catalytic sections was modelled at 100 kW pilot scale [34]. The project extensively investigated the liquid-fed SDE, including SO_2 crossover induced by electro-osmotic drag caused by the movement of protons and its impact on H_2 production efficiency [35]. Gold-coated stainless steel bipolar plates were also evaluated to enhance acid resistance and cell performance [36]. Building on these studies, Gasik et al. [37] developed and evaluated a liquid-fed, platinum-group-metal-free SDE stack under ambient pressure, providing design guidelines. Process simulation is reported by Guerra-Niehoff et al. [15], as discussed above. Liberatore et al. [38] reported LCOH of 9.3–16 €/kg for a 100 % renewable energy supply based on multi-objective optimisation.

The EU-Pegasus project [39], which ran from 2016 to 2021, also aimed to advance sulphur-process-related technologies. However, it is not included in Table S1 in the Supplementary File because the project focused primarily on sulphur production and combustion following the H_2SO_4 dissociation and SO_3 splitting process. In addition to the international collaborative projects, several advanced research studies have been reported by Chen et al. [40] and Zeng et al. [41], focusing on material selection, numerical modelling and analysis, experimental investigations, and prototype validation of H_2SO_4 splitting reactors.

Despite the numerous advantages associated with solar-driven HyS cycles and the extensive experimental and numerical research conducted on their development, the concept has yet to achieve commercialisation, even at the demonstration plant scale. Primary barriers to further commercialisation include the insufficient technological maturity of key HyS cycle components, specifically the CST-integrated H_2SO_4 splitting reactor and the SDE, alongside a scarcity of detailed, component-level financial data reflecting actual industrial operating conditions. Therefore, the EU-HySelect project [42] (2023–2026), as listed in Table S1 in the Supplementary File, aims to take the next step towards commercialisation by constructing, testing, and analysing the first ever—to the best of the authors' knowledge—solar-driven HyS demonstration plant. Unlike the previous volumetric solar receiver-reactor, this demonstration plant employs the centrifugal solar particle receiver (fourth-generation CST system [10], also used in the EU-Pegasus project), which enables more stable and high-temperature heat transfer using heated particles. A prior work by Lanchi et al [43]. conducted process simulation and energy analysis of several solar-driven HyS process concepts, including industrial practices, to identify which concepts offer energy efficiency benefits.

The work presented here is part of the EU-HySelect project. Its primary objective is to perform the TEA of the HyS demonstration plant's solar thermal and thermochemical subsystems, addressing technical challenges and providing practical financial data to advance the HyS cycle from TRL 4–5 to 6–7 (hereinafter, this plant is referred to as HySelect solar thermal-thermochemical demonstration plant). The actual cost data are essential for verifying concepts in demonstration plants and mitigating inaccuracies common in commercial-scale projections. The novelty of this study lies in the first demonstration-scale TEA of a solar-driven HyS plant, employing a detailed component-level costing methodology. Importantly, this work studies experimental demonstration plants with unavoidable inflexible options, not optimal or cost-competitive designs.

2. HySelect plant concept

2.1. Concept description

Fig. 1 shows a simple block diagram of the entire HySelect plant concept.

As shown in Fig. 1, there are seven key blocks: (0) Concentrated solar particle system, (1) H_2SO_4 dissociation and SO_3 splitting reactor system, (2) Gas separation system A, (3) Gas separation system B, (4) Gas separation system C, (5) SDE system, and (6) Acid concentration system. The main idea of the concept plant is to separate the solar thermal-thermochemical part i.e. mainly the H_2SO_4 splitting section, which includes Blocks 0, 1, 2, and 3, from the chemical-electrochemical part i.e. mainly the SDE section, which includes Blocks 4, 5, and 6. The H_2SO_4 splitting section is installed in a solar tower with a receiver with an appropriate heat transfer medium. In this study, solid particles are used, although other media, such as air or absorbing gases, could also be employed [44]. On the other hand, the SDE section would ideally be located within an existing industrial H_2SO_4 plant. Within the framework of the EU-HySelect project, the solar thermal-thermochemical section is based in Jülich, while the chemical-electrochemical section is located in Duisburg, Germany.

The purpose of Block 0 is to heat the particles within the solar cavity receiver (an enclosed receiver that absorbs concentrated solar radiation while minimizing thermal losses), located at the top of the solar tower, to temperatures exceeding 1173 K using concentrated solar thermal

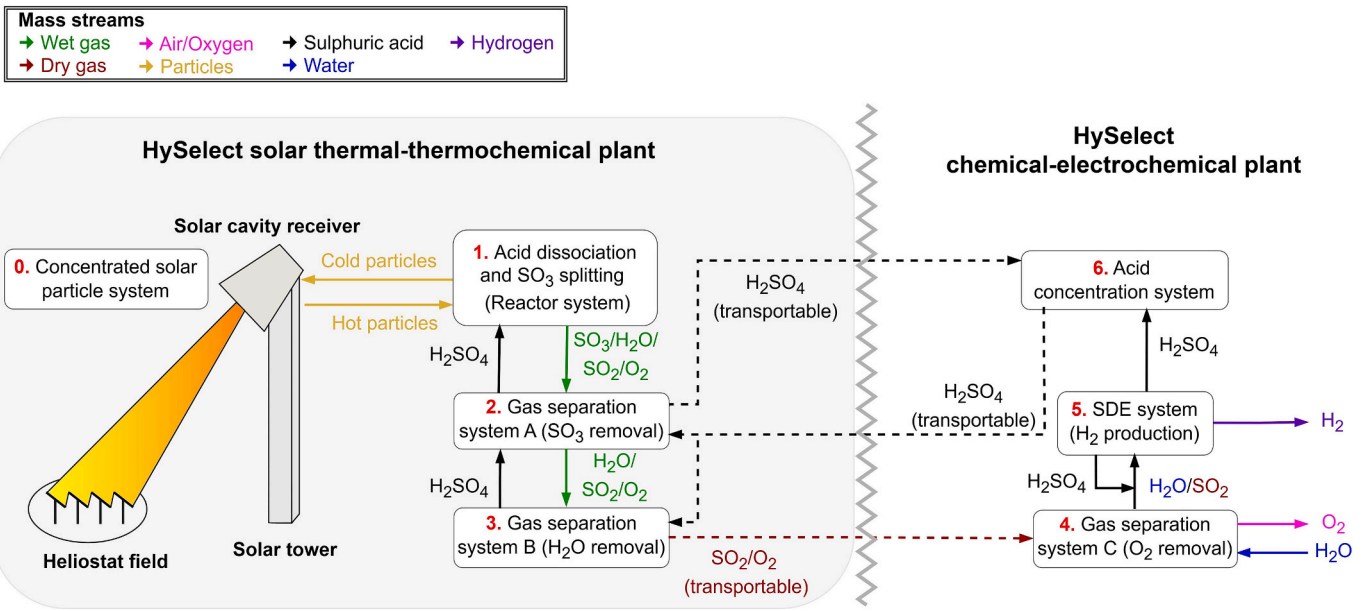

Fig. 1. Simple block diagram describing the HySelect plant concept. The plant is conceptualised into seven key process blocks, categorised into two primary sections: (1) the solar thermal-thermochemical section and (2) the chemical-electrochemical section. This study focuses on the analysis in Section (1).

energy collected by heliostats (a vast field of mirrors). The heated particles are subsequently used to transfer heat to the H_2SO_4 splitting reactor in Block 1. After releasing their thermal energy, the cooled particles are recirculated to the solar receiver, where they are reheated before re-entering the process. In Block 1, the thermal energy supplied from Block 0 drives both H_2SO_4 dissociation and SO_3 splitting reaction, yielding SO_2 and O_2 as products. Block 2 is a gas separation system to separate SO_2 and O_2 gases from SO_3, H_2O, SO_2 and O_2 gas mixture which is produced from Block 1. Concentrated H_2SO_4 is transported from the HySelect chemical-electrochemical plant (Block 6), mixed with secondary flows to produce H_2SO_4 at a specified concentration, and fed to Block 1. Part of this stream is shipped back to the HySelect chemical-electrochemical plant. A possible heat recovery system is considered in this block. The separated SO_2 and O_2 gas mixture (containing some amount of H_2O) is sent to Block 3. In this block, the SO_2 and O_2 gas mixture is first dried by using the concentrated H_2SO_4 transported from the HySelect chemical-electrochemical plant, followed by compression to enable transport back to the chemical-electrochemical plant for further processing. The spent H_2SO_4 is sent to Block 2, where it is mixed with concentrated H_2SO_4 to form H_2SO_4 at a specified concentration. As mentioned in the introduction, this paper focuses on the energy demand and cost analysis of the HySelect solar thermal-thermochemical demonstration plant (Blocks 0 to 3) from the practical real-world application perspective, generating solar SO_2 as the first, intermediate product. Nevertheless, for a complete picture, the material flows of the chemical-electrochemical part are briefly presented below.

At the chemical-electrochemical part of the HySelect plant, the transported SO_2 and O_2 gas mixture is first separated using the principle of water absorption in Block 4. The SO_2 dissolved in water is then mixed with H_2SO_4 and sent to Block 5 to produce H_2 through the SDE process. The required electric power for SDE can be provided either from a solar PV system or a CSP system. The produced H_2 is separated from diluted H_2SO_4 stream in Block 5, and this diluted H_2SO_4 is sent to Block 6 for further concentration. The demonstration-scale TEA results of the HySelect plant's chemical-electrochemical subsystems (Blocks 4 to 6) will be presented in the forthcoming second paper.

2.2. Qualitative analysis of HyS concept decoupling

The proposed decoupled HyS architecture separates the process into two distinct operational zones to optimise both industrial integration and resource utilisation. This physical separation facilitates a modular design that offers several qualitative advantages over fully integrated, monolithic HyS plants, particularly concerning site selection and infrastructure use.

A primary advantage of this modularity is the potential for industrial symbiosis with existing chemical infrastructure. By isolating the chemical-electrochemical section, the system can be retrofitted into established H_2SO_4 manufacturing plants. This approach allows for the efficient reuse of critical industrial assets, including existing gas treatment facilities, safety protocols, and designated explosion-proof areas. Furthermore, this integration minimizes the need for new land acquisition and allows the system to leverage existing power grid connections and cooling water loops, significantly reducing the capital risks associated with "greenfield" development.

Beyond industrial integration, the decoupled architecture affords greater flexibility in resource management, specifically regarding solar irradiance and water consumption. Because the thermal decomposition process is physically separated from the electrolysis loop, the high-temperature solar field can be sited independently in optimal, solar-rich regions without being constrained by the location of a chemical hub. Furthermore, the separation of these loops enables a reduction in water intensity; by isolating the H_2SO_4 concentration system, the design minimises the water requirements typically associated with large-scale acid concentration devices. This modularity ensures that the cycle can operate efficiently even in arid environments where solar resources are abundant but water is scarce.

Regarding the logistics of transporting H_2SO_4 and SO_2, both chemicals are already routinely transported over long distances by the existing H_2SO_4 industry. In compliance with the stringent safety regulations associated with the chemical industry [45], the separated thermochemical and electrochemical facilities can be connected using these established transport routes. Consequently, linking the geographically distinct modules would involve minimal environmental or political impact, leveraging mature infrastructure to connect the separate operational zones.

Finally, it is important to emphasise that the current study serves as a foundational test case to demonstrate the feasibility of the decoupled concept at the demonstration scale. While the qualitative benefits are evident, a comprehensive validation is required to quantify the potential

of this decoupling strategy. To explicitly quantify the benefits of this decoupling strategy at a demonstration scale, a forthcoming study will focus specifically on the HyS chemical-electrochemical demonstration plant. While the current manuscript addresses the solar thermal-thermochemical section, this companion paper will analyse the chemical-electrochemical components. Together, these two studies will provide a comprehensive, quantitative TEA of the full decoupled demonstration plant. Ultimately, a third study will address commercial-scale deployment by incorporating specific geographic location selection and transportation logistics, enabling a quantitative comparison between the proposed decoupled architecture and fully integrated concepts.

2.3. Operational risks and mitigation strategies

This section outlines the operational risks and corresponding mitigation strategies applicable to the proposed HyS solar thermal-thermochemical demonstration plant. Because the demonstration plant processes H_2SO_4, its risk profile and safety protocols align closely with those of conventional commercial H_2SO_4 production plants. In terms of general safety, H_2SO_4 facilities typically exhibit a moderate hazard potential within the chemical industry, owing to well-established engineering controls, stringent regulatory oversight, and standardised safety management systems [46]. This assessment is supported by data from the U.S. Environmental Protection Agency (EPA) Office of Emergency Management, which indicates that petroleum and refining facilities experience Risk Management Plan (RMP)-reportable accident rates approximately four times higher than those of chemical manufacturing facilities including the H_2SO_4 facilities. In this context, the accident rate is defined as the number of unique facilities experiencing accidents per sector divided by the total number of unique facilities in that sector [47]. Additionally, the U.S. National Toxic Substance Incidents Program recorded H_2SO_4 involvement in 3.0 % (236 of 7,990) of single-chemical fixed-facility incidents between 2010 and 2014 [48]. Given the well-understood reaction chemistry of H_2SO_4 and established safety engineering practices, major maintenance intervals for these facilities typically average 2–2.5 years [49].

Among serious accident scenarios in H_2SO_4 plants, SO_2 and SO_3 leaks pose significant human health and environmental hazards. Most facilities mitigate this risk by operating at slightly negative pressure relative to ambient conditions, aiming to prevent outward leakage. Nevertheless, Occupational Safety and Health Administration (OSHA) assessments indicate that this approach alone is inadequate, necessitating additional mechanical integrity safeguards [50]. In addition, an automated pressure control system originally developed by Sumitomo Metal Mining Co., Ltd. (now in the public domain following patent expiration) can be employed to mitigate pressure fluctuations within processing pipelines, thereby preserving the intended negative-pressure regime and reducing the risk of its loss [51].

As discussed above, H_2SO_4 production facilities are generally less susceptible to catastrophic runaway reactions than petrochemical plants. However, these facilities handle significantly higher concentrations of corrosive chemicals compared to many other industrial operations. In particular, the materials and catalysts employed in the H_2SO_4 splitting reactor require careful selection, and numerous studies are currently underway to enhance their durability and service life. Badini et al [52]. investigated the corrosion behavior of SiC-based laminates at 1123 K for 1000 h in an atmosphere simulating the harsh conditions of the SO_3 splitting reaction. Despite the formation of new phases, four-point bending tests revealed that the flexural modulus remained virtually unchanged, while the flexural strength actually increased. Agrafiotis et al. [53] conducted long-term testing (100–950 h) of catalyst-coated SiC honeycombs under the harsh conditions of the SO_3 splitting reaction at 1123 K. Their study demonstrated stable SO_3 conversion rates for approximately 300 h using Iron (III) oxide (Fe_2O_3) powder-coated Silicon-Infiltrated Silicon Carbide (SiSiC) honeycombs, and extended stability to roughly 550 h for in-house synthesized $Fe_{0.7}Cr_{1.3}O_3$-coated SiSiC honeycombs. In a study of short-term testing (25 h) at 1123 K, Zeng et al. [54] identified Copper (Cu)-Aluminum (Al) and Cu-Fe as the most effective catalysts for coating the SiC honeycomb structure. These coatings sustained SO_3 conversion rates above 84 % and 74 %, respectively, while exhibiting negligible deactivation of the conversion rate ($<$ 1 %).

3. Methodology

3.1. Process simulation approach

The process of the HySelect solar thermal-thermochemical demonstration plant was modeled using Aspen Plus V14 in steady-state mode. The simulation was developed by defining the process flowsheet, selecting an appropriate thermodynamic model, specifying operating conditions, validating key unit models, and performing mass and energy balance calculations. The following assumptions and constraints define the boundary conditions of the demonstration plant:

- The mass flow rate of inlet H_2SO_4 stream is adjusted in Block 1 so that 0.12 mol/s of SO_2 is produced. This amount of SO_2 is required as an input to the electrochemical plant to achieve the targeted H_2 production of 0.11 mol/s as the objective of the HySelect demonstration plant in line with the Key Performance Indicators of the Clean Hydrogen Partnership Joint Undertaking Strategic and Innovation Agenda 2021–2027 [55].
- A solar centrifugal particle receiver with 80 % receiver efficiency (based on Buck and Sment [56]) is used to collect the required thermal power for the splitting reactor and TES.
- A particle TES is also considered at the demonstration plant, which should store twice the thermal power needed for the H_2SO_4 splitting process. Twice the thermal power was selected as a design point to enable the operation of H_2SO_4 splitting process outside daylight hours (e.g., 8–16 h full load operation of particle storage depending on daytime operating hours).
- The H_2SO_4 splitting section is operating at a slight underpressure compared to ambient to prevent escape of toxic SO_2 and SO_3 gases in the event of a malfunction, as is usual industrial practice for such splitting reactors. The slight underpressure is achieved by means of a simple blower placed at the end (cold) of the splitting process.
- The outlet gas temperature of the H_2SO_4 reactor system is set to 1073 K.
- A factor of 0.75 is applied on the equilibrium conversion rate in Eq. (2) to account for realistic operation e.g. due to catalyst degradation [53].
- A spray tower system (direct contact heat exchange) is used instead of a heat exchanger (indirect contact heat exchange) to cool and condense the hot acid gas flow emitted from Block 1. The spray tower system generally avoids the corrosion due to the high gas and H_2SO_4 temperature and the generation of acid mist, which is difficult to separate [2], and it is the method of choice in conventional gas cleaning systems. Therefore, this spray tower system is currently in operation for this purpose in Grillo Chemicals GmbH, the industrial partner of the consortium owning and operating such units.
- The volume flow rates of the gas and liquid entering the spray tower are adjusted to meet the technical requirements of the tower for proper separation, as provided by Grillo Chemicals GmbH.
- The overall pump efficiency was assumed to be 75 % [57]. In addition, the isentropic and mechanical efficiencies of the compressor were assumed to be 85 % and 95 %, respectively [58,59]. Finally, the overall efficiency of the motor driving the vertical particle transport system was assumed to be 80 % [60].
- The maximum temperature of the H_2SO_4 pump is 423 K.
- The target concentration of H_2SO_4 circulating in the HySelect solar thermal-thermochemical demonstration plant is more than 90 wt%.

This is because, for commercially available austenitic stainless steel (AISI types 304, 310, 316, 317, 321, and 347), a highly concentrated H_2SO_4 ($\geq$ 90 wt%) is less corrosive than H_2SO_4 with concentrations ranging from 50-90 wt%. Especially, the corrosion is significant when the acid concentration is 50 wt% [61]. In addition, the amount of heat required for the H_2SO_4 splitting process is less compared to diluted H_2SO_4 with a higher water content.

- 93 wt% Of H_2SO_4 is shipped from the HySelect chemical-electrochemical demonstration plant to supply 90 wt% acid to Block 1. The value of 93 wt% was chosen since it is one of the values of commercially available H_2SO_4 products (66 Degree Baume H_2SO_4) [62], and it can be easily sourced from existing acid plants if necessary. Moreover, concentrations exceeding 93 wt% were not employed to avoid the significant increase in energy penalty associated with the H_2SO_4 concentration block in the HySelect chemical-electrochemical demonstration plant
- A single-stage water/lithium bromide absorption chiller is used in the HySelect solar thermal-thermochemical demonstration plant in order to effectively utilize the low grade waste heat within the plant which otherwise would be discharged. An absorption chiller module with a Coefficient of Performance (COP) of 0.71 is considered in this study. The COP value was determined based on discussions with supplier companies.
- An ammonia (R717)-based vapour compression refrigeration system is integrated into the process to meet additional cooling demands. A COP of 6.348 and an evaporation temperature of 280 K are assumed in this study [63].

3.2. Thermodynamic model

In the Aspen flowsheet for the HySelect solar thermal-thermochemical demonstration plant, the property method ElecNRTL is chosen for most of the unit blocks. However, it is known that this electrolyte model has stability issues at temperatures above 573 K. To solve this problem, the H_2SO_4 properties model was divided into two temperature ranges based on 573 K. Above 573 K, the aqueous dissociation equilibria of H_2SO_4 was replaced with a nonvolatile complex-forming equilibrium. The details are shown in Gorensek and Summers's work [14].

Realistic thermodynamic models of acid systems, especially ternary [SO_3-H_2O-H_2SO_4] system, are of great interest for practical process simulations of the HySelect solar thermal-thermochemical demonstration plant. Therefore, the thermodynamic models of such systems were adjusted based on previous work. The model of SO_3-H_2O-H_2SO_4 ternary system was modified based on the work from Que et al. [64]. Their thermodynamic model is valid over a whole concentration range from pure SO_3 to pure H_2O to pure H_2SO_4 with the temperature up to 773 K. It mainly targets the accurate prediction of the performance in the acid splitting section. Here, the thermodynamic properties that the model can accurately predict include the liquid–liquid equilibrium, vapour-liquid equilibrium, and calorimetric properties. The equations governing the liquid–liquid equilibrium and vapour-liquid equilibrium are listed below [64].

$$f_i^{\alpha} = f_i^{\beta}. \tag{5}$$

$$Py_i\varphi_i = x_i\gamma_i f_i^{0}. \tag{6}$$

here, P represents the system pressure, f_i^0 shows the liquid fugacity of pure component i at the system temperature and pressure, y_i is the mole fraction in the vapour phase, φ_i shows the fugacity coefficient in the vapour phase, x_i represents the mole fraction in the liquid phase, and γ_i is the activity coefficient in the liquid phase. The two superscripts α and β represent the two different liquid phases. Presented below is the equation for the excess enthalpy, a key calorimetric property essential for determining the heats of mixing, dilution, and solution.

$$H^E = -RT^2\left(\sum\nolimits_m x_m\frac{\partial \ln\gamma_m}{\partial T} + \sum\nolimits_i x_i\frac{\partial \ln\gamma_i}{\partial T}\right). \tag{7}$$

here, R is the gas constant and T is the temperature. The two subscripts m and i represent the molecular species and ionic species, respectively. Further details regarding the thermodynamic equations are provided in the study by Que et al [64].

3.3. Key parameter validation for the H_2SO_4 splitting reactor

This section presents the validation of the Aspen model for the H_2SO_4 splitting reactor based on two key parameters: (1) conversion ratio of SO_3 catalytic splitting process and (2) thermal power demand of H_2SO_4 dissociation (Eq. (1)) and SO_3 splitting processes (Eq. (2)). The experimental data for the first key parameter were obtained from the study by Agrafiotis et al. [53] and Zeng et al. [54]. On the other hand, the experimental data for the second key parameter were obtained from the study by Chen et al. [40], who tested the first H_2SO_4 splitting reactor prototype operating under high-temperature, high-pressure helium conditions. The model validation focused exclusively on the H_2SO_4 splitting reactor, as it represents the most emerging and critical component of the proposed process. The remaining components, including the compressor, absorption chiller, and vapour compression refrigeration system, are conventional industrial units with well-established performance characteristics. Consequently, uncertainties associated with these components were assessed through the sensitivity analysis presented in a later section. Regarding the concentrated solar particle receiver, its performance was not directly validated because the present work is based on steady-state process simulation.

Fig. 2 shows the Aspen Plus simulation results of the conversion ratio for SO_3 splitting processes, compared with theoretical and experimental values reported in the literature. The SO_3 conversion ratios evaluated in this study at equilibrium (at 0.1 and 1 MPa) and under practical application (applying a 0.75 coefficient, at 0.1 MPa) are represented by a solid line and a dashed line, respectively. The equilibrium conversion rates (at 0.1 and 1 MPa) reported by Corgnale et al. [65] are shown as dots. The experimental SO_3 conversion rates at 0.1 MPa reported by Agrafiotis et al. [53] are plotted as black inverted triangle for commercial Fe_2O_3 powder-coated SiSiC honeycomb and "x" for the in-house synthesised $Fe_{0.7}Cr_{1.3}O_3$-coated SiSiC honeycomb. Furthermore, the experimental conversion rates reported by Zeng et al. [54] are plotted as blue squares for Cu-Al coated SiC honeycombs and triangles for Cu-Fe coated ones. The experimental values represent the average values obtained for the Fe_2O_3, $Fe_{0.7}Cr_{1.3}O_3$, Cu-Al, and Cu-Fe catalysts over testing periods of 300, 600, 25, and 25 h, respectively. The Weight Hourly Space Velocity (WHSV), shown in Fig. 2, is defined as the ratio of the feed mass flow rate to the catalyst mass.

The comparison of the conversion rates at 0.1 MPa and 1 MPa indicates that higher operating pressures adversely affect the conversion rates of the SO_3 splitting reaction. Moreover, Fig. 2 shows that our simulation model using Aspen Plus can predict the SO_3 conversion rate with good accuracy (with an error of less than 1 % compared to the theoretical results reported by Corgnale et al.). Finally, from Fig. 2, it can be seen that applying a coefficient of 0.75 to the equilibrium conversion rate is a reasonable assumption when compared with the experimental values reported by Agrafiotis et al., particularly those from the Fe_2O_3 catalyst. The experimental data reported by Zeng et al. show values close to the equilibrium conversion rate, particularly when the Cu-Al catalyst is used. In this study, the practical SO_3 catalytic conversion rate at 1123 K and 0.1 MPa was determined to be 0.63. This compares with Agrafiotis et al., who reported rates of 0.60 for Fe_2O_3 and 0.70 for $Fe_{0.7}Cr_{1.3}O_3$, and Zeng et al., who observed rates of 0.84 for Cu-Al and 0.74 for Cu-Fe.

Fig. 3 shows the Aspen Plus simulation results for the thermal power demand of H_2SO_4 dissociation and SO_3 splitting processes, benchmarked

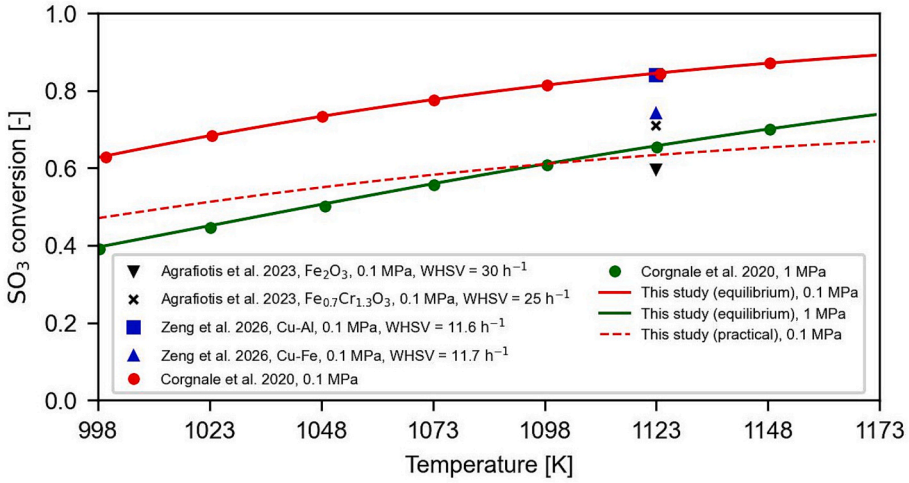

Fig. 2. Aspen Plus simulation results of the conversion ratio for SO_3 splitting process, compared with theoretical and experimental values reported in the literature. The theoretical results were adopted from Corgnale et al. [65], whereas the experimental results were obtained from Agrafiotis et al. [53] and Zeng et al. [54]. The experimental data shown in black inverted triangle and "x" represent the performance of SiSiC honeycomb structures coated with commercially available Fe_2O_3 and in-house synthesized $Fe_{0.7}Cr_{1.3}O_3$. The experimental data shown in blue square and triangle represent the performance of SiC honeycomb structures coated with Cu-Al and Cu-Fe. The WHSV is defined as the ratio of the feed mass flow rate to the catalyst mass. (For interpretation of the references to colour in this figure legend, the reader is referred to the web version of this article.)

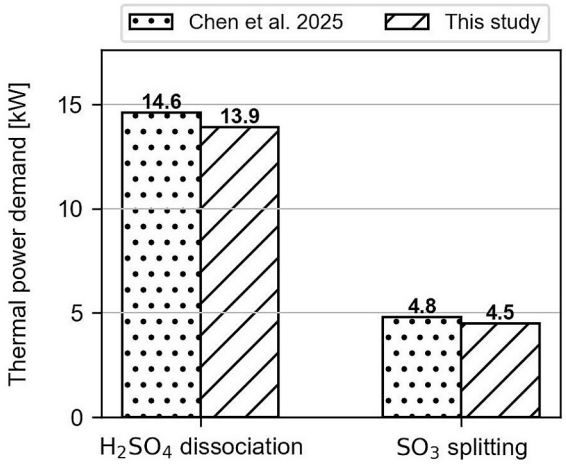

Fig. 3. Aspen Plus simulation results for the thermal power demand of H_2SO_4 dissociation and SO_3 splitting processes, benchmarked against experimental data provided by Chen et al. [40]. The inlet temperature of 290 K, inlet pressure of 0.3 MPa, H_2SO_4 mass flow rate of 14 kg/h, H_2SO_4 concentration of 98 wt%, and average SO_3 splitting conversion ratio of 0.7 were used as operating conditions for the validation work.

against experimental data provided by Chen et al. [40]. The validation was performed using the following operating conditions: inlet temperature of 290 K, inlet pressure of 0.3 MPa, H_2SO_4 mass flow rate of 14 kg/h, H_2SO_4 concentration of 98 wt%, and average SO_3 splitting conversion ratio of 0.7 (this corresponds to an O_2 production rate of 1.1 Nm^3/h or a H_2 production rate of 2.2 Nm^3/h). The detailed descriptions of the experimental setup and corresponding Aspen Plus process flowsheet are provided in the study by Chen et al.

Fig. 3 illustrates that the thermal power demand for H_2SO_4 dissociation exceeds that of SO_3 splitting, primarily due to the inclusion of H_2SO_4 evaporation. Approximately 75 % of the total thermal power demand is used for H_2SO_4 dissociation in both cases. Furthermore, Fig. 3 shows a strong correlation between the simulation results of this study and the experimental data reported by Chen et al. [40]. The relative deviations (or absolute deviations) from the experimental results are 4.8 % (0.7 kW_{th}) for H_2SO_4 dissociation and 6.3 % (0.3 kW_{th}) for SO_3 splitting.

3.4. Cost estimation for the demonstration plant

For the cost estimation of the HySelect solar thermal-thermochemical demonstration plant, a bottom-up approach was adopted. In the bottom-up approach, the fixed capital investment is estimated from purchased equipment costs using installation factors to account for direct and indirect capital expenses. The operating costs are determined by estimating fixed Operation and Maintenance (O&M) costs as a fraction of the fixed capital investment, while variable O&M costs are calculated based on detailed process mass and energy balances. In this study, the total investment cost of the demonstration plant was defined as the sum of the fixed capital investment and the operating costs incurred during the demonstration period. A 6 h daily operation of concentrated solar particle receiver is considered, corresponding to a typical real day operation in the DLR solar tower facility in Jülich, allowing for soft start-up and shut-down. The operation for an additional 12 h is also considered by supplying heat from the hot particle storage tank. Furthermore, the demonstration plant is expected to operate for 120 days per year.

The purchased equipment costs are estimated prices as of January 2025. Chemical Engineering Plant Cost Index (CEPCI) for January 2025 was estimated at 793 based on published CEPCI trends reported by Chemical Engineering magazine and extrapolation from 2024 monthly values. Official numeric values were not publicly available at the time of analysis. The following formula was used to calculate the cost of the equipment at different scales and years:

$$EC = EC_{ref} \bullet \left(\frac{S}{S_{ref}}\right)^{d} \bullet \left(\frac{I}{I_{ref}}\right). \quad (8)$$

here, EC, S, and I are the equipment cost, characteristic capacity, and CEPCI, respectively. Furthermore, the subscript *ref* and superscript *d* are the reference year and equipment specific scale factor, respectively. The reference equipment cost, reference characteristic capacity, and equipment specific scale factor were obtained from the quotation data obtained and the list provided by Albrecht et al. [66], Townsend and Faber [67], Woods [68], and Sinnott and Towler [69]. Furthermore, the CEPCI value corresponding to the reference year was sourced from an online document provided by Maxell [70]. Given that the equipment cost

estimates were derived from a combination of vendor quotations and literature values, a ± 20 % uncertainty margin was applied to the total equipment cost, consistent with the approach of Townsend and Faber [67]. In addition, an uncertainty margin of ± 10 % was applied to the target year (2025) CEPCI. This uncertainty range was derived from the historical annual variation observed over the preceding 23 years.

The fixed capital investment includes direct plant and indirect plant costs. The direct plant cost consists of equipment, equipment and machine assembly, piping, insulation, electronic devices, measuring and control devices, buildings and equipment racks, foundations and ancillary construction work costs. In this study, an installation factor of 450 % of the total equipment cost was used to estimate the direct plant cost. The installation factor of 450 % is based on 530 % of surcharge applied for technical and fine chemical plants provided by Ullrich (the surcharge factor varies to account for the design concepts of different plants) [71]. The surcharge of 530 % was reduced to 450 % in consideration of industrial practices and reduction of surcharge for buildings, equipment racks, foundations, and ancillary construction work due to the existing infrastructure (i.e., solar tower and heliostat field). On the other hand, the indirect plant cost includes engineering and supervision cost, as well as cost related to regulatory initiatives. This price was estimated at 10 % of direct plant cost based on industrial practices and surcharge data provided by Ullrich [71]. The estimation methodology for the installation factor, along with the referenced literature, remains commonly employed in current industrial practices. Consequently, the adoption of these approaches is appropriate for analysing the cost structures of specific technical and chemical plants, including those at the demonstration plant scale (i.e., HySelect solar thermal-thermochemical demonstration plant).

The O&M cost includes the fixed cost and variable cost. The fixed O&M cost covers personnel, maintenance and repair, and tax and insurance costs. The personnel cost comprises salaries, benefits, and training expenses for operators, engineers, technicians, and administrative personnel. The cost was calculated based on the three assumptions made: (1) a monthly gross salary of 4,732 €/employee (values relating to 'manufacturing' were cited from 2024, as the 2025 data were not publicly available at the time of the analysis [72]), (2) a non-wage labour cost of 28 % [73], and (3) 10.5 full-time equivalent employees in the plant. The calculated annual salary was reduced to an amount equivalent to 120 working days, with the final personnel cost amounting to 5 % of the fixed capital investment. The maintenance and repair cost refers to the total expenses incurred for regular maintenance (such as filter replacement and periodic inspections) and inventory costs for spare parts. The cost was estimated based on the study by Schemme [73] and represents 3.6 % of the fixed capital investment. The tax and insurance cost was estimated based on the study by Schemme [73] and represents 3.2 % of the fixed capital investment. With regard to the variable O&M cost, it includes transportation, electricity, wastewater costs. The transportation cost was estimated by using a specific transportation cost of 6.5 €/km based on quotations received. In the estimation, a single standard articulated truck (length < 16.5 m, width < 2.55 m, height < 4.0 m, load capacity < 40 tons) was considered for the transportation [74]. The electricity cost was calculated based on the electricity rate of 18.25 ct/kWh (estimated based on Germany's industrial electricity rate, excluding reductions, for February 2025 provided by the German Federal Network Agency [75]). The wastewater cost represents the cost of wastewater treatment, and the total cost was simply calculated using the cost of 2 €/m^3 reported by Albrecht et al. [66].

4. Aspen plus process flowsheet and system description

4.1. Concentrated solar particle system (Block 0) and H_2SO_4 dissociation and SO_3 splitting system (Block 1)

Fig. 4 shows the Aspen flowsheet for concentrated solar particle system (Block 0) and H_2SO_4 dissociation and SO_3 splitting system (Block 1), with all flow paths colour-coded and labelled. Here, the lower half of the figure illustrates Block 0, while the upper half depicts Block 1. Furthermore, the flow numbers "000A-P" and "000B-P" are identical but not directly connected to each other in order to avoid the convergence problem in the Aspen Plus simulation.

Beginning with Block 0, the heat exchanger unit "SOL-REC" refers to a centrifugal particle receiver. This unit belongs to a concentrated solar thermal system that includes a heliostat field and a solar tower. The centrifugal particle receiver uses both centrifugal force from rotation and gravity to create a particle flow. This concept usually uses a hollow cylindrical cavity structure (such as a drum) [11], and rotation causes a

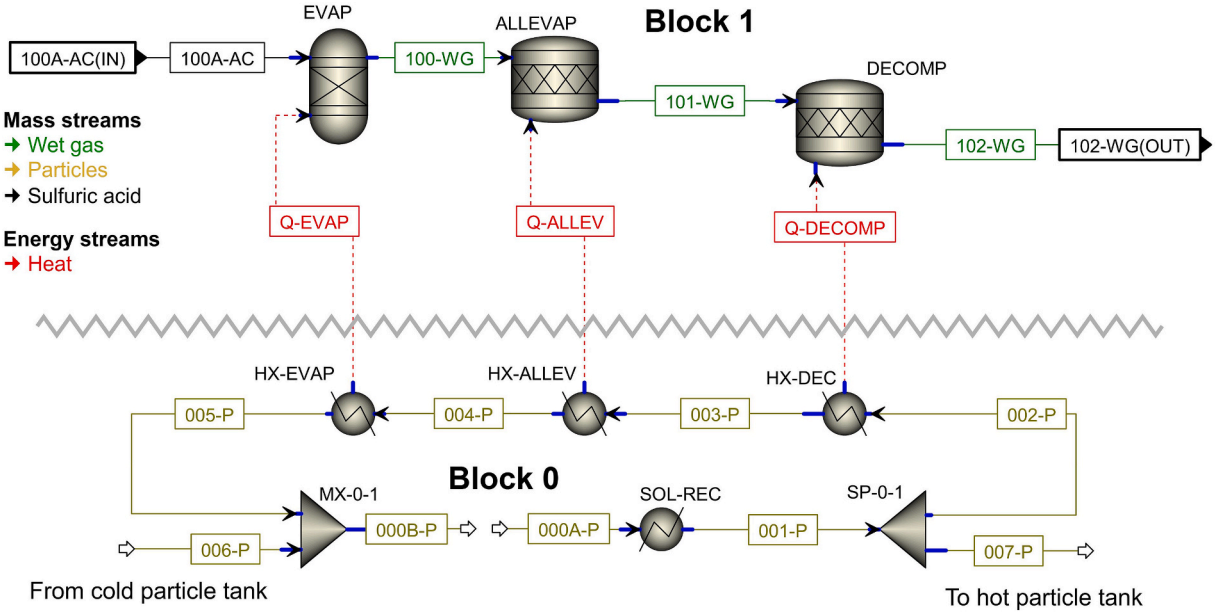

Fig. 4. Aspen flowsheet for concentrated solar particle system (Block 0) and H_2SO_4 dissociation and SO_3 splitting system (Block 1). The lower half of the figure illustrates Block 0, while the upper half depicts Block 1. The thermal energy is transferred from the particles in Block 0 to the H_2SO_4 acid splitting reactor in Block 1, as shown in the heat stream ("Q-EVAP", "Q-ALLEV", "Q-DECOMP").

dense particle film to form on the entire inner surface of this structure. The particle film moves downward while receiving concentrated sunlight directly. By adjusting the angular velocity of the receiver, it is possible to control the residence time of the particles. Fig. 5 shows the centrifugal particle receiver [76] installed in the DLR solar tower facility in Jülich, Germany. A heliostat field that concentrates sunlight, along with the HEHTRES facility equipped with the particle transport and storage system and H_2SO_4 splitting reactor, are also shown in the figure. The performance calculation of the heliostat field is not included in this model, but the thermal power required for the receiver is calculated based on the aforementioned assumptions and constraints of the demonstration plants. The aperture diameter, drum diameter, length, and nominal thermal power of the centrifugal particle receiver are 1.13 m, 1.6 m, 2.3 m, and 1 MW_{th}, respectively.

After passing through the "SOL-REC" unit, the heated particles flow ("001-P") is split and particles equivalent to two-thirds of the absorbed thermal power ("007-P") are stored in the high temperature TES tank. The particles that do not enter the TES tank ("002-P") pass through the H_2SO_4 splitting reactor ("HX-EVAP"="EVAP", "HX-ALLEV"="ALLEV", "HX-DEC"="DECOMP") for transferring thermal power within the particles to the H_2SO_4 dissociation and SO_3 splitting units ("Q-EVAP", "Q-ALLEV", "Q-DECOMP"). This is explained in detail in Fig. S1 in the Supplementary File, which shows the detailed 3D CAD drawing of the HEHTRES facility planned to be employed for the HySelect solar thermal-thermochemical demonstration plant. The particles passing through the H_2SO_4 splitting reactor ("005-P") are mixed with particles from cold storage unit ("006-P"), and the mixed particles are recirculated to the "SOL-REC" unit via a lift system ("000B-P" = "000A-P").

In Block 1, "EVAP" is the RGibbs reactor model that is able to simultaneously calculate phase and chemical equilibrium. It describes the first step of acid splitting (Eq. (1)). "ALLEVAP" and "DECOMP" are the RStoic reactor model that is the simplest of all Aspen Plus's reactor type. "ALLEVAP" considers the dissociation of unconverted H_2SO_4 after the "EVAP" unit. Although this reaction might occur inside the SO_3 splitting reactor, this unit is separated from "DECOMP" unit to avoid the complexity of process simulation. At the temperature and pressure of 998 K and 0.1 MPa, all of the H_2SO_4 is converted into SO_3, as shown in Fig. S2 of the Supplementary File. "DECOMP" considers the second step of H_2SO_4 splitting (Eq. (2)). The conversion rate of SO_3 to SO_2 depends on the operating temperature and pressure. The lower the pressure and the higher the temperature, the higher the conversion rate obtained as shown in Fig. 2.

4.2. Gas separation system A (Block 2)

Fig. 6 (a) shows the entire Aspen flowsheet for gas separation system A (Block 2), while Fig. 6 (b) shows the detailed Aspen flowsheet of "SPRAY" block shown in Fig. 6 (a). All streams are colour-coded and labelled. The Block 2 follows a layout copied from the real operation practice of the H_2SO_4 industry. Two spray towers are used in this block: (i) spray tower for acid condensation ("SPT-AC") and (ii) spray tower for water condensation ("SPT-W"). The purpose of the spray tower (i) is to spray liquid H_2SO_4 to condense SO_3 and remove it from the SO_2 and O_2 gas mixture. On the other hand, the objective of the spray tower (ii) is to spray liquid water to reduce the water content of the SO_2 and O_2 gas mixture. Here, the flow numbers "209-AC" and "212-AC" indicate the raw materials transported from and to the HySelect chemical-electrochemical demonstration plant, respectively.

Flow "102-WG" indicates the high-temperature wet acid gas provided by Block 1. This wet gas is cooled down to 623 K in the gas–gas heat exchanger "HX-2–1". The air flow "200A-AIR" is used for cooling, and the heat extracted here is recovered within the system. The recovered heat is to be used for a small-capacity single-stage absorption chiller. The temperature of 623 K was set to account for the dew point of H_2SO_4 and SO_3, which can lead to damage of the heat exchanger due to corrosion [2]. The cooled wet acid gas "200-WG" flows to the first spray tower "SPT-AC" as a gas flow. The "SPT-AC" is a "RadFrac" unit without condenser and reboiler and can be used as an absorption tower unit. Since Aspen Plus does not list a unit model that can be used as a spray tower, the "RadFrac" unit was used to simulate spray tower performance. In addition, the gas flow and liquid flow provided for the spray tower were divided into two ("201-WG" and "202-WG" for gas streams and "206-AC" and "207-AC" for liquid streams, respectively) due to the specific design of the tower. Unlike the counter-current type, the flow of gas and spray liquid enters from the top of the tower and exits from its bottom. This design allows for longer gas residence time and more efficient mixing of gas and liquid. By splitting the gas and liquid flows and considering two spray systems in one absorption tower, it is possible to predict performance similar to that of the spray tower used by Grillo Chemicals GmbH. The temperature in the spray tower was adjusted to

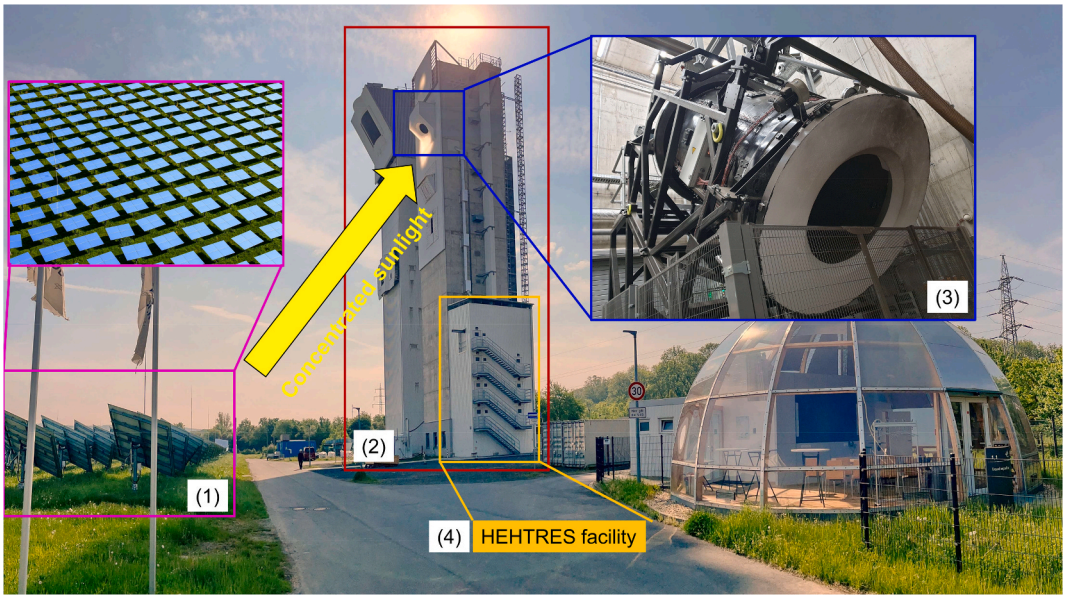

Fig. 5. DLR centrifugal particle receiver installed in the solar tower facility in Jülich, Germany. (1) heliostat field, (2) two solar towers, (3) 1 MW_{th} scale centrifugal particle receiver, and (4) HEHTRES facility including the particle transport and storage system and acid splitting reactor.

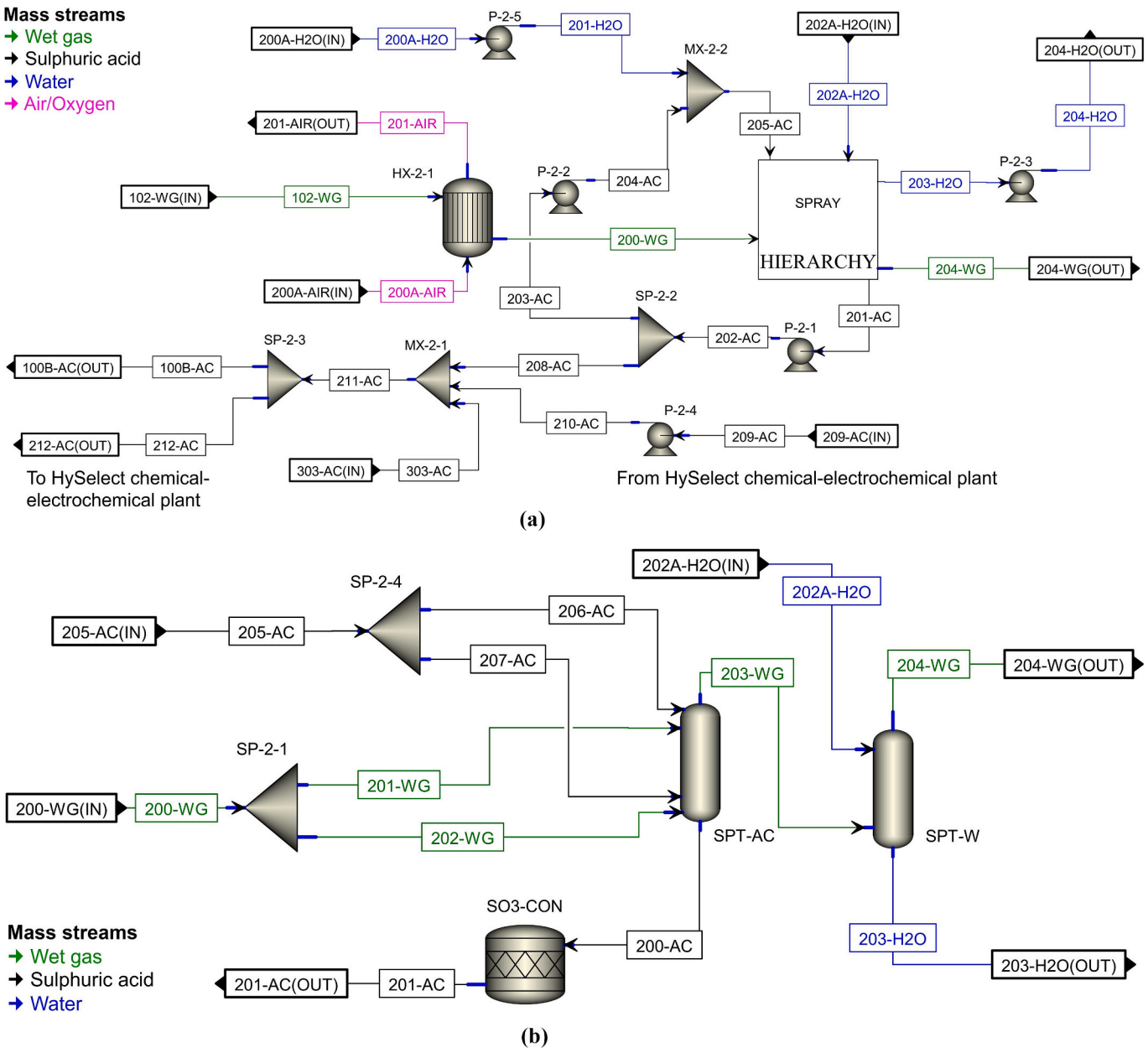

Fig. 6. Aspen flowsheet for gas separation system A (Block 2). (a) complete Aspen flowsheet, (b) detailed Aspen flowsheet of "SPRAY" block. The gas–gas heat exchanger (HX-2–1) and the two spray towers (SPT-AC and SPT-W) are the principal components of Block 2, and their arrangement is consistent with industrial operating practices in H_2SO_4 production.

maintain 423 K.

The sprayed liquid captures SO_3 from the acid vapour, and the acid liquid containing SO_3, H_2SO_4, and H_2O is discharged from the bottom of the spray tower as "200-AC". The SO_3 condensation, that occurs inside the spray tower, is considered in the RStoic reactor model "SO3-CON". The diluted H_2SO_4 "201-AC" is recirculated to the H_2SO_4 splitting section "208-AC" and to the spray tower "203-AC". H_2SO_4 of 93 wt% concentration is pumped ("209-AC") and diluted H_2SO_4 which is coming from Block 3 ("303-AC") are mixed with the flow "208-AC" to adjust the acid concentration, and the mixed H_2SO_4 solution "211-AC" is separated again to adjust the mass flow rate of the flow towards Block 1 ("100B-AC" and "212-AC"). The flow "100B-AC" is recirculated to the H_2SO_4 splitting section (Block 1), while the flow "212-AC" is transported to the HySelect chemical-electrochemical demonstration plant. The H_2SO_4 liquid stream "203-AC" is pressurised at 0.15 MPa for the spray flow, and it is mixed with 0.15 MPa water containing a small amount of SO_2 ("201-H2O"). The mixed H_2SO_4 solution "205-AC" is then split and sent back to the first spray tower.

The gases containing SO_2, O_2, and H_2O ("203-WG") are sent to the second spray tower ("SPT-W") for condensation of the water content. Since the spray tower considered here is of a counter-current type, a regular "RadFrac" unit without a condenser or reboiler is used. Unlike the first spray tower, the second spray tower uses 0.15 MPa water containing a small amount of SO_2 ("202A-H2O") as the spray solution. The condensed stream containing H_2O and a small amount of SO_2 ("203-H2O") is discharged from the second spray tower via the pump. The wet gas stream from the second spray tower, "204-WG", is sent to the gas separation system B (Block 3), described in the next section.

4.3. Gas separation system B (Block 3)

Fig. 7 shows the Aspen flowsheet for the gas separation system B

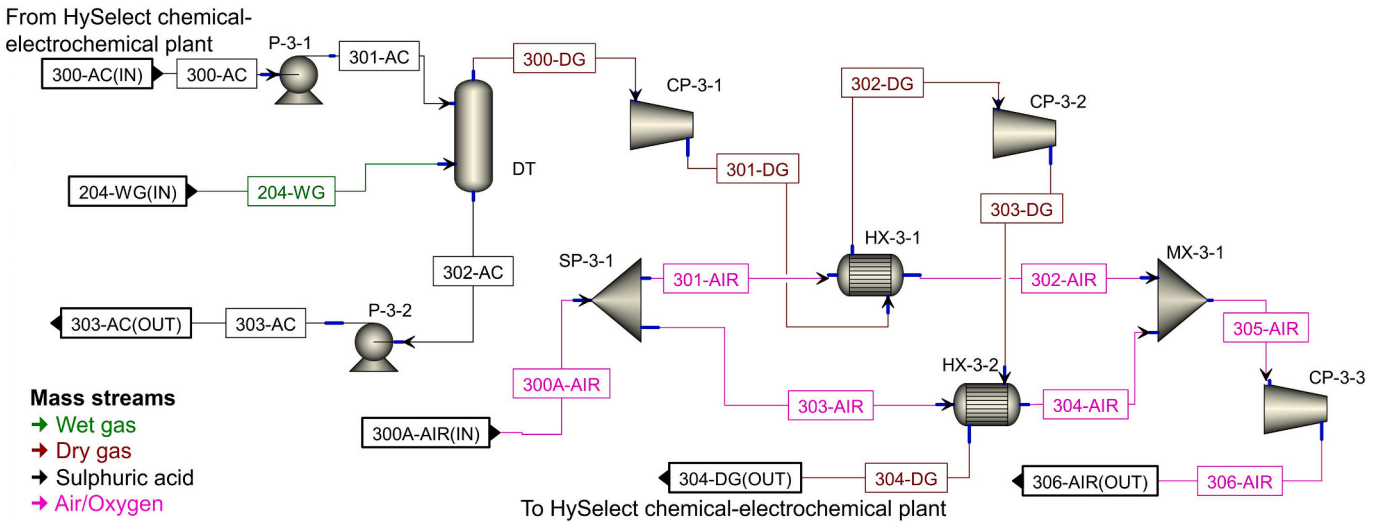

Fig. 7. Aspen flowsheet for gas separation system B (Block 3). The key components of this block are the dry tower "DT" and the gas compressors ("CP-3–1" and "CP-3–2"), which dry, partially condense, and compress the SO_2 and O_2 gas mixture prior to shipment.

(Block 3), with all flow paths colour-coded and labelled. The purpose of this block is to dry and compress the SO_2 and O_2 gas mixture, ready for transportation. Here, the flow numbers "300-AC" and "304-DG" denote the raw material transported from and the product transported to the HySelect chemical-electrochemical demonstration plant, respectively.

Flow "204-WG" indicates the SO_2 and O_2 gas mixture supplied from the gas separation system A. Since this mixture is still a wet gas (contains a small amount of H_2O), the gas stream must first be dried before compression. This procedure is performed by a commercially available packed absorption column. Therefore, a regular "RadFrac" unit without a condenser or reboiler is used for the absorption column "DT". H_2SO_4 of 93 wt% concentration transported from the HySelect chemical-electrochemical demonstration plant is used as a liquid stream ("300-AC") to condense the water in the SO_2 and O_2 gas mixture. A diluted H_2SO_4 "302-AC" is discharged from the bottom of the absorption column via the pump. The dry SO_2 and O_2 gas mixture "300-DG" is sent to the rotary screw gas compressor "CP-3–1". The stream "300-DG" is first compressed to 0.35 MPa ("301-DG"), and sent to the gas–gas heat exchanger "HX-3–1" to remove the heat generated during the compression. The compressed air "301-AIR" is used to cool the hot gas mixture. The cooled gas mixture "302-DG" is then sent to the second rotary screw gas compressor "CP-3–2" and is compressed at 1.3 MPa ("303-DG"). The compressed gas is sent to the gas–gas heat exchanger "HX-3–2" where it is cooled by heat exchange with compressed air "303-AIR". The cooled compressed gas mixture "304-DG" is finally stored in a gas container (as shown in Fig. S3 in the Supplementary File) and transported to the HySelect chemical-electrochemical demonstration plant. The used air streams ("302-AIR" and "304-AIR") are mixed ("305-AIR"), and compressed at the same pressure as "300A-AIR". The compressed air stream ("306-AIR") is cooled by the chilled water and recirculated back into the system. The Aspen flowsheet for the overall process, including the absorption chiller block, is provided in the Supplementary Material. In addition, the complete stream tables, property package settings, convergence criteria, and key design parameters related to the Aspen Plus simulation are provided therein.

5. Results and discussions

5.1. Cost analysis of the demonstration plant

Table 2 shows the equipment costs for the HySelect solar thermal-thermochemical demonstration plant. The equipment ID shown in the table can be referenced from Fig. 4, Fig. 6, Fig. 7, and Figs. S4–S5 in the Supplementary File. The reference equipment cost, reference characteristic capacity, equipment specific scale factor, and reference CEPCI used in each equipment cost calculation are provided in Table S2 of the Supplementary File. In addition, corresponding power demand of each components used for the cost calculation are summarised in Table S3 in the Supplementary File.

In Block 1, the components related to particles are listed. As mentioned previously, "SOL-REC" refers to a 1 MW_{th} centrifugal particle receiver. The cost was estimated based on considering a partial load operation of the receiver (300 kW_{th}) and the equation proposed by Buck and Sment [56]. "HX-DEC", "HX-ALLEV", and "HX-EVAP" in the demonstration plant to be built, are all integrated in a single H_2SO_4 splitting reactor, following the typical vertical tube evaporator (or vertical shell and tube heat exchanger) design developed in EU-Project Pegasus [39]. The cost of the H_2SO_4 splitting reactor was based on the price estimated in EU-Project Pegasus and the equipment specific scale factor of 0.55 (for vertical long tube evaporator) provided by Sinnott and Towler [69]. The total heat transfer area of the reactor/heat exchanger was used as characteristic capacity. Although it is not shown in the flowsheet, the price of the vertical particle transport system (240 kW_{th} scale), hot and cold tank storage systems (160 kW_{th} scale), and bauxite particles was also calculated. All prices were estimated based on the equation provided by Reiner and Stefano [77]. Furthermore, the following assumptions were made for each equipment:

- Vertical particle transport system: A mine hoist system that includes two skips, one hoist, and OLDS elevator (for the recovery of particle leakage) is considered. The lift height is set to 50 m. Furthermore, the particle mass flow rate and temperature (during lifting) were calculated by Aspen, yielding values of 0.352 kg/s and 623 K, respectively.
- Hot and cold tank storage systems: A cylindrical container with a height (2.70 m) twice the diameter (1.35 m) of the cylinder is considered. In addition, the particle temperatures in the hot tank and cold tank are set to 1173 K and 623 K, respectively.
- Bauxite particles: Particles with a specific heat capacity of 1200 J/(kg K), a bulk density of 2000 kg/m^3, and specific cost of 1 €$_{2018}$/kg are considered. Moreover, the additional 3 % of the total particle mass is considered to account for spillage of the particle during the 120 days operation.

It is important to note that the cost of the solar tower facility and heliostat field has not been considered in this study. This is because these

Table 2
Equipment cost breakdown in the HySelect solar thermal-thermochemical demonstration plant. The equipment ID can be referenced from Fig. 4, Fig. 6, Fig. 7, and Figs. S4–S5 in the Supplementary File. The purchased equipment costs were estimated based on prices as of January 2025. The "Literature" and "Company quotation" columns provide the source references for the cost data of each piece of equipment.

Block number	Equipment ID	Price in $€_{2025}$	Specification	Literature	Company quotation
1	SOL-REC	83,000	1 MW_{th} centrifugal particle receiver in a partial load operation (300 kW_{th}).	[56]	–
	HX-DEC, HX-ALLEV, HX-EVAP	253,000	80 kW_{th} acid splitting reactor.	[39] and [69]	–
	Out of flowsheet	300,000	240 kW_{th} vertical particle transport system.	[77]	–
	Out of flowsheet	39,000	6.912 GJ (1.92 MWh) hot and cold tank storage systems.	[77]	–
	Out of flowsheet	10,000	Bauxite particle.	[77]	–
2	HX-2–1	13,000	Acid gas–gas heat exchanger.	[66]	Received
	P-2–1	5,000	H_2SO_4 pump.	[66]	Received
	P-2–2	5,000	H_2SO_4 pump.	[66]	Received
	P-2–3	2,000	Water pump.	[66]	–
	P-2–4	4,000	H_2SO_4 pump.	[66]	Received
	P-2–5	1,000	Water pump.	[66]	–
	SPT-AC	100,000	Acid spray column.	–	Received
	SPT-W		Water spray column.		
3	DT		Bubble tray column.		
	P-3–1	2,000	H_2SO_4 pump.	[66]	Received
	P-3–2	2,000	H_2SO_4 pump.	[66]	Received
	CP-3–1, HX-3–1 CP-3–2, HX-3–2	60,000	2-stage gas compressor.	–	Received
	CP-3–3	5,000	Air compressor.	[66]	–
	Out of flowsheet	2,000	Gas scrubber vessel.	–	Received
	Out of flowsheet	10,000	End-gas blowers, Vacuum for upstream system.	–	Received
	Out of flowsheet	52,000	Gas container (capacity of 0.9 m^3), 13 items.	–	Received
AC	HX-AH, HX-AC	11,000	Absorption chiller.	–	Received
	CP-AC-1	6,000	Air compressor.	[66]	–
	HX-AC-1	10,000	Liquid-gas heat exchanger (finned tube heat exchanger).	[67]	–
	HX-AC-2	10,000	Liquid-gas heat exchanger (finned tube heat exchanger).	[67]	–
	HX-AC-3	negligible	Liquid-liquid heat exchanger, (flat plate heat exchanger).	[66]	–
	P-AC-1	2,000	Water pump.	[66]	–
	HX-CL-P	29,000	Vapour compression refrigeration system.	[68]	–
	Out of flowsheet	21,000	Cooling tower.	[69]	–
	Out of flowsheet	25,000	Intermediate bulk container for 90 wt% liquid H_2SO_4 (capacity of 1 m^3) made of stainless steel with a PTFE liner, 5 items.	–	Received
Total equipment cost		1,062,000			

facilities have already been constructed in Jülich, Germany, and the concept for the demonstration plant is to utilise existing infrastructure.

In Block 2, the equipment mainly related to the acid stream are listed. "HX-2–1" is a gas–gas heat exchanger used for high-temperature exhaust gas from Block 1. "P-2–1", "P-2–2", and "P-2–4" are the H_2SO_4 pumps. These equipment costs were estimated based on supplier quotations and the equipment costs data provided by Albrecht et al. [66]. "P-2–3" and "P-2–5" are the water pump and the cost was estimated based on the equipment costs data provided by Albrecht et al. [66]. The costs for the column systems that include "SPT-AC", "SPT-W", and "DT (in Block 3)" were estimated based on supplier quotations.

In Block 3, the equipment mainly related to gas compression are listed. "P-3–1" and "P-3–2" are the H_2SO_4 pumps and the cost was estimated based again on supplier quotations and the equipment costs data provided by Albrecht et al. [66]. "CP-3–1", "HX-3–1", "CP-3–2", "HX-3–2" are considered as 2-stage gas compressor, and the cost was estimated based on quotations. "CP-3–3" is an air compressor and the cost was estimated based on the equipment costs data provided by Albrecht et al. [66]. Although it is not shown in the flowsheet, the prices of the gas scrubber vessel, end-gas blowers, 13 gas containers were similarly estimated based on quotations received. The gas scrubber vessel is only used during the shutdown process, which lasts for about one hour per operating day, to avoid the emission of SO_2 gas from the plant. The end-gas blowers are used to evacuate the upstream process during the shutdown process and remove the remaining gas in the pipes and vessels. The gas containers store a mixture of compressed SO_2 and O_2, and are used to transport this to the HySelect chemical-electrochemical demonstration plant.

Regarding the AC block, the cost of absorption chiller was estimated based on quotations received. The costs for "CP-AC-1", "HX-AC-3", and "P-AC-1" were estimated based on the equipment costs data provided by Albrecht et al. [66]. The costs for "HX-AC-1" and "HX-AC-2" were calculated based on the equipment costs data provided by Townsend and Faber [67]. The cost for "HX-CL-P" was estimated based on the equipment costs data provided by Woods [68]. Although not depicted in the flowsheet, a cooling tower is incorporated into the plant to cool the condenser water for the absorption chiller and vapour compression refrigeration system, reducing the temperature from 303–308 K to 298–303 K. The cost of the cooling tower was estimated based on the equipment costs data provided by Sinnott and Towler [69]. In addition,

four intermediate bulk containers are considered, that store a liquid H_2SO_4 (90 wt%) and are used for the same purpose as gas containers. Since the containers must be able to withstand 90 wt% H_2SO_4, stainless steel with a Polytetrafluorethylen (PTFE) liner is considered as the material. The costs of these containers were estimated based on quotations received.

Based on the calculated total equipment cost, the total investment cost of the demonstration plant is calculated as mentioned in Section 3.4. Table 3 shows the results for the HySelect solar thermal-thermochemical demonstration plant. The cost analysis results include not only fixed capital investment, but also variable O&M cost (electricity, water, etc.) and fixed O&M cost (i.e., personnel, maintenance and repair, and tax and insurance) based on 120 days of experimental operation of the demonstration plant (operates for 6 h using solar heat and 12 h using stored heat per day).

As described in Section 3.4, an installation factor of 450 % of the total equipment cost was applied to estimate the direct plant cost. However, the costs associated with the particles and the vertical particle transportation system were excluded from the total equipment cost and instead added directly to the total direct plant cost, as they were treated as bulk material inventory and a fully integrated subsystem, respectively. The indirect plant cost was calculated by applying a factor of 10 % to the direct plant cost. The personnel, maintenance and repair, tax, and insurance costs included in the fixed O&M costs, as well as the transportation, electricity, and wastewater costs included in the variable O&M costs, were estimated based on the assumptions presented in Section 3.4. The transportation cost represents the cost required to transport thirteen gas containers (for storing compressed SO_2 and O_2 gas mixtures) and five intermediate bulk containers (for storing 90 wt% liquid H_2SO_4) to the HySelect chemical-electrochemical demonstration plant in Duisburg, Germany (this is equivalent to a distance of approximately 75 km one way). Using a specific transportation cost of 6.5 €/km, the daily transportation cost for thirteen gas containers and five intermediate bulk containers was estimated at 487.5 €. The electricity cost represents the total cost of electricity used by pumps, compressors, vapour compression refrigeration, absorption chiller, and vertical particle transportation.

A sensitivity analysis was conducted on the equipment costs and the CEPCI for the target year (2025) to assess the associated cost uncertainty. Based on the uncertainty margins described in Section 3.4, nine uncertainty scenarios were evaluated by varying the equipment cost and CEPCI uncertainties: (A) [0 %, 0 %], (B) [20 %, 0 %], (C) [−20 %, 0 %], (D) [0 %, 10 %], (E) [20 %, 10 %], (F) [−20 %, 10 %], (G) [0 %, −10 %], (H) [20 %, −10 %], and (I) [−20 %, −10 %], where each pair represents [equipment cost uncertainty, CEPCI uncertainty]. The analysis results indicated that the highest total investment cost occurs in Scenario (E), amounting to 6.1 million $€_{2025}$, whereas the lowest total investment cost occurs in Scenario (I), amounting to 3.4 million $€_{2025}$. Further details are provided in Fig. S6 of the Supplementary Material.

The cost analysis has revealed that the total cost of the demonstration plant is 4.7 million $€_{2025}$ (Minimum: 3.4 million $€_{2025}$, Maximum: 6.1 million $€_{2025}$) and the main costs of the demonstration plant are direct plant costs. Of the equipment costs, those related to the solar particle heating process are the highest in the demonstration plant, followed by the column systems, 2-stage gas compressor, thirteen gas containers for compressed SO_2 and O_2 gas mixtures, vapour compression refrigeration system, five intermediate bulk containers for storing 90 wt % liquid H_2SO_4, cooling tower, acid gas–gas heat exchanger, and absorption chiller. Since the centrifugal solar particle receiver system (with TES) and the H_2SO_4 splitting reactor represent innovative components of the HySelect solar thermal–thermochemical plant, they offer substantial potential for cost reduction through economies of scale. This is particularly relevant because these components account for a significant share of the overall equipment costs, meaning that cost reductions at larger plant scales could substantially decrease the total plant cost. The centrifugal solar particle system, representing a fourth-generation high-temperature solar thermal technology [10], still faces financial-related challenges to further commercialisation. Nevertheless, recent advances in materials science and engineering are contributing to the development of more compact and cost-effective systems, including TES technologies capable of providing heat at high temperatures [78]. Consequently, the centrifugal solar particle system is expected to play an important role in reducing the cost of high-temperature heat supply while contributing to the long-term decarbonisation of industrial heat. In contrast, the technological maturity of the H_2SO_4 splitting reactor is currently lower than that of the solar particle receiver system. However, its relatively low technology readiness level also indicates substantial potential for further technological development and cost reduction. In particular, the financial barriers associated with H_2SO_4 splitting reactor are expected to decrease as a result of continued technological advancement and the growing number of international and national research and development projects as described in Section 1. These developments are expected to accelerate technology maturation, improve economic feasibility, and enhance the potential contribution of H_2SO_4 splitting reactor to future solar thermochemical energy systems. Lastly, while the vertical particle transportation system accounts for a significant portion of the capital cost in the demonstration plant, this proportion is expected to decrease at larger scales, as the required tower height does not increase proportionally with plant capacity.

Table 3
Total investment cost of the HySelect solar thermal-thermochemical demonstration plant. The "Literature" and "Industrial verification" columns indicate the source of the cost estimates, distinguishing between values obtained from the literature and those derived from industrial practice based on communications with industry partners.

Category	Item	Price in $€_{2025}$	Specification	Literature	Industrial verification
Capital investment					
	Direct plant cost	3,694,000	Installation factor of 450 % of the total equipment cost	[71]	Yes
	Indirect plant cost	369,400	Factor of 10 % of direct plant cost	[71]	Yes
Variable O&M					
	Transportation cost	58,500	Specific tranportation cost of 6.5 €/km by a single standard articulated truck	–	Yes
	Electricity cost	3,000	Germany's industrial electricity rate in February 2025 of 18.25 ct/kWh (without reductions).	[75]	No
	Wastewater cost	negligible	Specific wastewater cost of 2 €/m^3	[66]	No
Fixed O&M					
	Personnel	255,000	Assumed monthly gross salary of 4,732 €/employee, non-wage labour cost of 28 %, 10.5 full-time equivalent employees	[72] and [73]	No
	Maintenance and repair	146,000	Factor of 3.6 % of fixed capital investment	[73]	No
	Tax and insurance	130,000	Factor of 3.2 % of fixed capital investment	[73]	No
Total demonstration plant cost		4,655,900			

5.2. Specific energy of solar SO_2 production

Table 4 shows the specific energy of solar SO_2 production at the HySelect solar thermal-thermochemical demonstration plant. The value is also compared to other results reported in other studies on HyS plants. Here, the specific energy of solar SO_2 production is calculated by the following equation:

$$e_{SO_2} = \frac{(\dot{Q}_{acid}/\eta_{rec}) + (W_{acid}/\eta_{PP})}{\dot{m}_{SO_2}}. \quad (9)$$

where, $\dot{m}_{SO_2}$ is the mass flow rate of SO_2 produced from the plant, $\dot{Q}_{acid}$ is the total thermal power needed for the H_2SO_4 dissociation and SO_3 splitting processes, η_{rec} is the solar receiver's thermal efficiency, W_{acid} is the total electric power needed in the solar thermal-thermochemical subsystem, and η_{PP} is the power cycle efficiency (assumed equal to 50 %). The thermal efficiency of the selected solar receiver has been explicitly incorporated into the specific energy calculation to account for the performance characteristics of the chosen receiver concept. Conversely, the efficiency of the heliostat field is deliberately excluded from this formulation.

It can be observed from Table 4 that the specific energy values obtained in this study are higher than those reported by Gorensek and Lanchi. The primary factors contributing to this are: (1) the absence of heat recovery for the inlet H_2SO_4 stream prior to the acid splitting reaction, (2) the maximum operating temperature constraint of the SO_3 splitting reaction, (3) the conservative assumption of the lowest SO_3 conversion rate, and (4) additional electrical power requirements for cooling. Notably, the significant difference arises from the extensive heat recovery applied to the inlet H_2SO_4 stream in the comparative study, contrasted with the additional electricity load for vapor compression refrigeration in the present work. In contrast, the specific energy values obtained in this work are higher than those reported by Guerra-Niehoff. This is primarily attributed to the use of a higher acid concentration and the efficiency of the solar receiver. When the mass fraction of H_2SO_4 is high, the mass fraction of water decreases, thereby the evaporation energy decreases in the process. The total amount of SO_2 generated is the lowest in this study, due to the size of the actual demonstration plant to be built, compared to theoretical full size plant studies.

Differing from the studies by Guerra-Niehoff and Gorensek, H_2SO_4 splitting temperatures exceeding 1123 K were not considered in this work. This limitation was imposed by the operating temperature constraints of the catalyst [65] as well as material concerns especially for the splitting reactor and heat recovery/gas separation system dealing with high temperatures and corrosive media. Furthermore, as in the study by Lanchi et al., this work did not assume equilibrium SO_3 conversion, as this condition has not yet been experimentally verified even at the laboratory scale [53]. Despite the advantages of indirect heat recovery demonstrated in the studies by Lanchi and Gorensek, this study excluded an internal heat recovery system to preheat the recirculated H_2SO_4. This decision was driven by the complexity of the acid gas–liquid heat exchanger, where simultaneous evaporation and condensation phenomena occur. Lastly, Gorensek's research considers a higher operating pressure of 1.41 MPa during the acid splitting process; however, given the significant health and safety concerns, certifications and applicable regulations, it is not common industrial practice to induce such a splitting reaction at pressures higher than ambient pressure as indicated in Section 2.3. The aforementioned facts demonstrate the importance of this research for practical industrial applications.

Nevertheless, a sensitivity analysis was performed to identify critical technologies and parameters capable of improving specific energy, independent of their current maturity levels. The sensitivity analysis investigated six parameters: (1) solar receiver efficiency (70–90 %), (2) SO_3 conversion rate (40–78 %), (3) maximum temperature in the SO_3 splitting reaction (1023–1123 K), (4) absorption chiller COP (0.65–0.84), (5) vapor compression refrigeration COP (5.0–7.5), (6) compressor isentropic efficiency (74–91 %). The sensitivity ranges were established based on literature data, previous model results, and manufacturer specifications. Specifically, the ranges for solar receiver efficiency, absorption chiller COP, and compressor isentropic efficiency were derived from studies by Buck and Sment [56], Santini and Dwyer [79], and Folkers et al. [59], respectively. The sensitivity bounds for the vapor compression refrigeration COP were selected using the manufacturer specifications [80]. The SO_3 conversion rate range was determined based on the work described in Section 3.3, with the upper bound representing the equilibrium conversion. Finally, the temperature range for the SO_3 splitting reaction was defined as $\pm$ 50 K relative to the baseline maximum temperature. The lower bound corresponds to the theoretical maximum dissociation (100 %) of H_2SO_4 to SO_3, based on the equilibrium conversion data in Fig. S2 in the Supplementary File, while the upper bound is defined by the material and catalyst constraints. Fig. 8 shows the results of the study. Here, note that the analysis assumes a fixed SO_2 production rate of 0.12 mol/s downstream of the H_2SO_4 splitting reactor, as defined in Section 3.1.

As illustrated in Fig. 8, the specific energy of solar SO_2 production is

Table 4
Specific energy of solar SO_2 production at the HySelect solar thermal-thermochemical demonstration plant. The specific energy values from other sources calculated using the same definition are also displayed.

Parameter	This study – HySelect demonstration plant	Guerra-Niehoff et al. [15]	Gorensek et al. [16]	Lanchi et al. [43]
Structure of the HyS plant	Divided into solar thermal part and electrochemical part	All processes are consolidated in single place	All processes are consolidated in single place	All processes are consolidated in single place
Solar receiver concept	Centrifugal solar particle receiver	Volumetric solar receiver-reactor	Indirect solar heating via high-pressure helium	Centrifugal solar particle receiver
Receiver efficiency	80 % [56]	40 % [28]	91 % [16]	80 % [56]
Applied thermal power to H_2SO_4 dissociation and SO_3 splitting process	80 kW_{th}	86 MW_{th}	353 MW_{th}	548 kW_{th}
Applied electric power	7.3 kW_{el}	2.2 MW_{el}	8.9 MW_{el}	21.1 kW_{el}
Mass fraction of H_2SO_4 in dissociation and SO_3 splitting process	90.0 wt%	62.5 wt%	90.0 wt%	76.8 wt%
Recirculated H_2SO_4 inlet temperature	332 K	417 K	466 K	564 K
Operating pressure in H_2SO_4 dissociation and SO_3 splitting process	0.1 MPa	0.1 MPa	1.41 MPa	0.1 MPa
Maximum temperature in H_2SO_4 dissociation and SO_3 splitting process	1073 K	1273 K	1123 K	1073 K
SO_3 conversion rate	58.3 %	94.6 %(at equilibrium)	62.3 %(at equilibrium)	59.8 %
Mass flow rate of SO_2 generated	26 kg/h	31 t/h	215 t/h	231 kg/h
Specific energy of solar SO_2 production	15.62 MJ/kg (or 4.34 kWh/kg)	25.20 MJ/kg (or 7.00 kWh/kg)	6.34 MJ/kg (or 1.76 kWh/kg)	8.24 MJ/kg (or 2.29 kWh/kg)

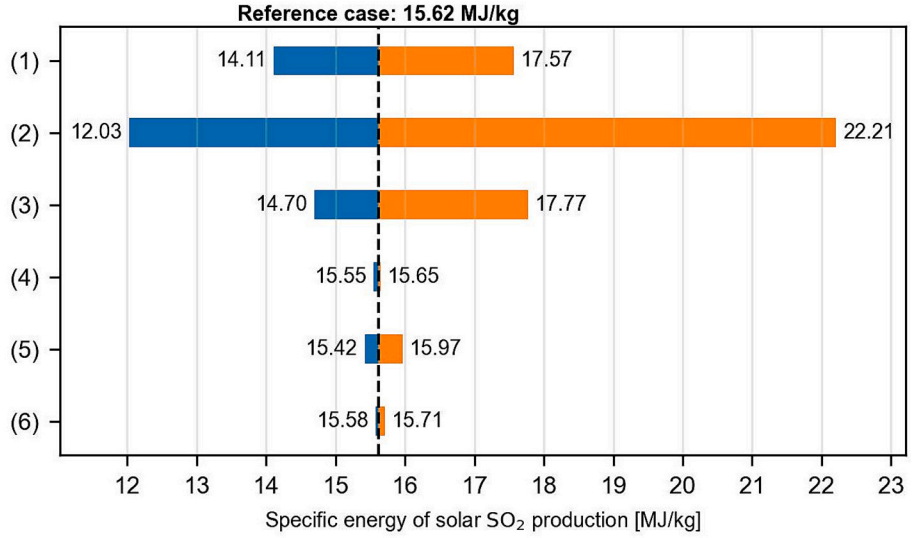

Fig. 8. Sensitivity analysis of specific energy of solar SO_2 production. Six parameters are investigated: (1) solar receiver efficiency [left bar: 90 %, right bar: 70 %], (2) SO_3 conversion rate [left bar: 78 %, right bar: 40 %], (3) maximum temperature in the SO_3 splitting reaction [left bar:1123 K, right bar: 1023 K], (4) absorption chiller COP [left bar: 0.84, right bar: 0.65], (5) vapor compression refrigeration COP [left bar: 7.5, right bar: 5.0], (6) compressor isentropic efficiency [left bar: 91 %, right bar: 74 %].

most sensitive to the SO_3 conversion rate, with the solar receiver efficiency and maximum SO_3 splitting reaction temperature ranking next in significance. The absorption chiller COP, vapor compression refrigeration COP, and compressor isentropic efficiency demonstrate considerably lower impact. The high sensitivity of the SO_3 conversion rate is attributed to its dual effect: it reduces the energy demand for H_2SO_4 splitting and simultaneously lowers the cooling load on the vapor compression refrigeration system. Higher conversion rates decrease the required mass flow rate of reactants (and water) to maintain the target SO_2 production rate of 0.12 mol/s, thereby reducing the electrical power needed for cooling. Similarly, solar receiver efficiency is critical as thermal power is the plant's primary driver. The maximum splitting reaction temperature is also a significant factor, as higher temperatures drive higher conversion rates. The practical conversion rate, which is defined as 75 % of the equilibrium rate, was applied to the analysis of this parameter. Based on these findings, specific energy was recalculated for the optimal scenario—maximising these three parameters: (1) solar receiver efficiency (90 %), (2) SO_3 conversion rate (85 %, corresponding to the equilibrium rate at 1123 K), and (3) maximum reaction temperature (1123 K). This configuration yielded the lowest specific energy of 10.15 MJ/kg (2.82 kWh/kg), which is substantially closer to the values reported by Gorensek and Lanchi, although it remains higher. This suggests that the internal heat recovery employed in their study to preheat the inlet H_2SO_4 stream has a significant impact on the overall specific energy.

In summary, the specific energy of solar SO_2 production in this study is less favourable than that reported by Gorensek and Lanchi, but more favorable than that reported by Guerra-Niehoff. The discrepancy with the values presented by Gorensek and Lanchi arises because incorporating practical plant considerations introduces energy penalties that are typically neglected in idealised literature models. Here, the term "practical" means that the process is operated at atmospheric pressure, that the maximum temperature in the H_2SO_4 splitting process is less than 1123 K, that the SO_3 conversion rate is lower than the equilibrium value, and conventional industrial equipment is used where possible. Once more, it is important to emphasise here that all equipment and technical solutions used in this process follow as close as possible current state-of-the-art conventional industrial practices. This is done to build a demonstration plant that closely follows existing designs to the maximum possible extent, thus minimizing risk and using where available "of-the-shelf" conventional equipment. Nevertheless, the sensitivity analysis was subsequently performed to pinpoint the technologies with the greatest potential to boost plant energy efficiency and drive further TRL advancement with a view to commercialisation. The findings identified three priority research directions: (1) optimizing solar receiver performance, (2) refining catalysts for higher SO_3 splitting conversion rates, and (3) developing heat- and corrosion-resistant materials to facilitate SO_3 conversion at elevated temperatures. Firstly, continued development and improved reliability of high-temperature solar thermal systems, also referred to as fourth-generation solar thermal systems [10], are essential for achieving the technological targets and advancing the solar-driven HyS plant toward commercialisation. Although several technological challenges remain, ongoing innovations in optical systems, materials, thermal energy storage, and system control are creating new opportunities to enhance system performance and reliability [9]. Secondly, improvements in catalyst performance, long-term durability, and the replacement of precious-metal catalysts with more abundant and cost-effective alternatives are essential for further increasing the TRL of the solar-driven HyS plant. As discussed in Section 1, substantial research efforts have already been undertaken, with many studies and development activities continuing to address these challenges. Finally, the development of materials with enhanced durability and corrosion resistance under the severe operating conditions of H_2SO_4 dissociation and SO_3 splitting is critical for further commercialisation of the solar-driven HyS cycle. Materials degradation in these highly corrosive environments represents a key technical challenge and is therefore an important area of research. As highlighted in Section 1, considerable research has already been conducted, and ongoing efforts continue to identify and develop materials capable of withstanding these demanding conditions.

5.3. *Pseudo Solar-to-H_2 efficiency*

This section details the pseudo solar-to-H_2 efficiency of the HyS solar thermal-thermochemical demonstration plant. The term "pseudo" is used because H_2 production is beyond the scope of this study; therefore, the H_2 production rate is estimated rather than numerically determined. Two cases are considered for the efficiency calculation: (1) base case, which is defined according to the boundary conditions specified in Section 3.1 and employs conventional industrial equipment; and (2) key-technology-matured case, in which the key technologies identified in the sensitivity analysis (Section 5.2) are assumed to have reached

maturity, while conventional industrial equipment is used for the remaining process components. The H_2 molar production rate is assumed to be 90 % of the SO_2 molar production rate in this study. Additionally, heliostat efficiency is incorporated into the solar-to-H_2 calculation. A value of 64 % is assumed for the base case, consistent with published data from the commercial cavity-type solar tower plant "Planta Solar 10" [81]. For the key-technology-matured case, an efficiency of 70 % is adopted, reflecting the upper limit reported by Corsi et al. [82] and Paul and Kedare [83]. The pseudo solar-to-H_2 efficiency, based on the H_2 LHV, is determined by the following equation.

$$\eta_{STH} = \frac{\dot{n}_{H2} LHV_{H2}}{(\dot{Q}_{acid}/(\eta_{rec} \bullet \eta_{helio})) + (W_{acid}/\eta_{PP})}. \quad (10)$$

where, $\dot{n}_{H2}$ is the expected molar flow rate of H_2 produced and η_{helio} is the heliostat efficiency. The obtained results are benchmarked against state-of-the-art solar thermochemical and electrochemical technologies reported in the literature, with the corresponding comparisons presented in Table 5. The solar thermochemical water-splitting cycles comprise the S-I three-step, copper-chlorine (Cu-Cl) four-step, and cerium oxide two-step processes. Conversely, the solar electrochemical hydrogen production relies on solar-coupled Solid Oxide Electrolysis (SOEL), Proton Exchange Membrane Electrolysis (PEME), and Alkaline Water Electrolysis (AWE).

Table 5 indicates that the S-I three-step and Cu-Cl four-step thermochemical cycles, along with the SOEL system, achieve relatively high solar-to-H_2 efficiencies. In contrast, the cerium oxide two-step cycle, PEME, and AWE systems demonstrate lower efficiencies. High-temperature processes are typically integrated with CST technology, whereas low-temperature processes are commonly coupled with solar PV systems. Electrolysis-based solar water splitting currently exhibits higher TRLs than solar thermochemical water splitting, which remains at a lower TRL. A comparison of the "pseudo" solar-to-H_2 efficiency reveals that the base case performance of the proposed system remains competitive with established technologies. Furthermore, the key-technology-matured scenario demonstrates substantial potential for large-scale hydrogen production from an energy efficiency perspective. It should be noted again, however, that this metric is termed "pseudo" because it excludes the auxiliary thermal energy required for H_2SO_4 concentration and the electrical energy consumed by the SDE process. The primary objective of this study is not to optimise thermodynamic efficiency or compete directly with other solar-driven water splitting routes; rather, it aims to quantify the economic viability and demonstrate the improvement potential of the first HyS demonstration plant concept. Consequently, the reported values should be interpreted cautiously and are not recommended for direct efficiency benchmarking against other technologies. A comprehensive analysis of the HyS electrochemical demonstration plant, including a rigorous determination of its true solar-to-H_2 efficiency, will be presented in a subsequent publication.

6. Conclusion

The steady-state energy demand and cost analysis of HySelect solar thermal-thermochemical demonstration plant were carried out. Aspen Plus was used to develop the flowsheet and perform the energy demand analysis. Four different blocks (i.e., Concentrated solar particle system, H_2SO_4 dissociation and SO_3 splitting system, Gas separation system A, and Gas separation system B) were considered in the process flowsheet. Based on the results of the energy demand analysis, the specific energy of solar SO_2 production was calculated and compared with literature values. Moreover, the pseudo solar-to-H_2 efficiency, derived from estimated production rates, was evaluated against current state-of-the-art benchmarks. In the cost analysis, financial figures for the actual experimental platform were determined using the results of the energy demand analysis, quotations, and equipment cost data provided in the literature. A sensitivity analysis was performed on the SO_2 specific energy and demonstration plant cost to evaluate parameter uncertainties and identify opportunities for TRL advancement.

The first key finding of this study is that the total cost of the

Table 5
Comparison of the calculated pseudo solar-to-H_2 efficiency against state-of-the-art solar thermochemical and electrochemical technologies. The considered benchmark technologies include the S-I three-step, Cu-Cl four-step, and cerium oxide two-step processes, as well as the SOEL, PEME, and AWE processes. Note: The efficiency value for the present study is designated as "pseudo" to reflect its preliminary nature; it should therefore be interpreted with caution as it represents a partial calculation rather than a complete system efficiency.

	Authors	Solar technology	Maximum process temperature	TRL	Solar-to-H_2 efficiency
Base case	This study	Solar tower	1073 K	4–5	14.6 %
Key-technology-matured case	This study	Solar tower	1123 K	4–5	24.3 %
S-I three-step cycle	Liberatore et al. [84]	Solar tower, Parabolic trough	1123 K	4–6 [85,86]	9.4–21.0 %
S-I three-step cycle	Yilmaz and Selbaş [87]	Solar tower	1123 K	4–6 [85,86]	32.7 %
S-I three-step cycle	Zeng et al. [88]	Solar tower, Parabolic trough, Linear Fresnel	1123 K	4–6 [85,86]	20.7 %, 16.1 %, 12.8 %,
Cu-Cl four-step cycle	Temiz and Dincer [89]	Parabolic trough	783 K	3–4 [85,86]	26.7 %
Cu-Cl four-step cycle	Khormi and Fronk [90]	Solar tower (particle-based and gas-based)	807 K	3–4 [85,86]	20.3 % (particle), 25.3 % (gas)
Cerium oxide two-step cycle	Sharma et al. [91]	Not specified	2150 K, 2370 K	2–4 [85]	6.5 %, 12.6 %
Cerium oxide two-step cycle	Lou et al. [92]	Not specified	1573 K, 1873 K	2–4 [85]	3.7 %, 13.7 %
SOEL	Mastropasqua et al. [93]	Parabolic dish	1173 K, 1373 K	5–7 [94]	13.2–16.1 %, 18.9–22.9 %
SOEL	Yadav and Banerjee [95]	PV, Parabolic trough	1273 K	6–8 [94]	10.1–15.9 %, 13.8–17.5 %
PEME	Calnan et al. [96]	PV	303 K	7–8 [94]	5.0–13.5 %
PEME	Arunachalam and Han [97]	PV	333 K	7–8 [94]	6.6–8.2 %
PEME	Niederhofer et al. [98]	PV	368 K	7–8 [94]	15.8–18.5 %
AWE	Calnan et al. [96]	PV	303 K	8–9 [94]	3.5–11.3 %

demonstration plant, which is equipped with a centrifugal solar particle receiver operating at a partial load of 300 kW_{th}, an 80 kW_{th} H_2SO_4 splitting reactor, and 6.912 GJ (1.92 MWh) of TES, reached 4.7 million $€_{2025}$ (range of uncertainty: 3.4–6.1 million $€_{2025}$). Regardless of their lower technology readiness levels, the centrifugal solar particle receiver and H_2SO_4 splitting reactor represent the most promising avenues for cost reduction at scale. This stems primarily from their significant contribution to total capital expenditure and the rapid advancements observed in both national and international research programs. Furthermore, the vertical particle transportation system represents a major capital expenditure component in the demonstration plant. However, its relative cost contribution is anticipated to diminish at commercial scales, given that tower height does not increase proportionally with throughput.

The second key finding of this study is that the specific energy of solar SO_2 production (at purity of 79.4 wt%, compressed at 1.3 MPa) in the proposed demonstration plant was 15.62 MJ/kg (or 4.34 kWh/kg). The results indicated that specific energy consumption exceeds values reported in most prior studies, primarily due to energy penalties arising from real-world plant constraints. These constraints include operating at slightly below atmospheric pressure, capping the H_2SO_4 splitting temperature at 1123 K, limiting SO_3 conversion to 75 % of equilibrium levels, and integrating standard industrial equipment. Additionally, the sensitivity analysis indicated that specific energy is most strongly driven by solar receiver efficiency, SO_3 conversion rate, and maximum reaction temperature, highlighting these as critical research priorities. Optimising these parameters reduced the specific energy to 10.15 MJ/kg (2.82 kWh/kg). Significant further reductions would require an internal heat recovery system that exploits the simultaneous evaporation and condensation of the inlet H_2SO_4 and outlet acid gas streams. This approach was deliberately omitted from the current analysis due to its engineering complexity, technical uncertainty, low maturity level, and the industry's preference for established methods.

The final key finding is that, despite partial solar-to-H_2 efficiency data prevents a straightforward comparison, both the base case and key-technology-matured scenario remain competitive with state-of-the-art solar thermochemical and electrochemical pathways. Full details on true solar-to-H_2 efficiency will be covered in a subsequent paper.

The main takeaway of this study is that integrating realistic industrial constraints yields less favorable specific energy values for solar SO_2 production than those reported in idealised literature models, which often neglect such practical considerations. However, the proposed plant model demonstrates greater potential for industrial implementation, as the equipment and technical solutions closely align with established industrial standards. Another key point is that the component-level cost data and total costs estimated in this paper (4.7 million $€_{2025}$, range of uncertainty: 3.4–6.1 million $€_{2025}$) can be used as reference values not only for future scale-up studies of HyS cycle plants, but also for the Solid Sulphur cycle and S-I cycle plants (all steps share the same H_2SO_4 splitting step). In addition, these cost data can be used in calculations and decision-making regarding future decarbonisation utilizing renewable heat in the H_2SO_4 industry. The final key takeaway is that future component-level research must prioritise CST technology and the H_2SO_4 splitting reactor, as these are critical bottlenecks with high potential for process optimisation of the HyS solar thermal-thermochemical demonstration plant. To facilitate further TRL advancement, validation efforts must specifically address the durability and lifetime of catalysts and materials used in the H_2SO_4 splitting reactor, alongside efficiency improvements for the solar particle receiver and integrated TES system.

Beyond the component-level analysis presented above, three future validation milestones are proposed to advance individual component research and increase the TRL of the solar-driven HyS cycle. First, a TEA of the HySelect chemical-electrochemical demonstration plant should be conducted to identify technical bottlenecks, establish financial cost data—particularly for the SDE process—and quantitatively assess the decoupling potential of the demonstration plant. Second, the energy demand analysis should be extended to transient operating conditions, including hourly variations in solar input, to better reflect real-world solar resource availability. Third, the TEA of the full HyS plant concept should be scaled to a commercial level using the technical and financial data obtained from the demonstration plant, thereby enabling an assessment of the LCOH and comparison with state-of-the-art solar-driven thermochemical and electrochemical technologies. The decoupling potential should also be validated at the commercial scale by comparing the decoupled configuration with the fully integrated HyS plant.

CRediT authorship contribution statement

Y. Kadohiro: Writing – original draft, Visualization, Validation, Software, Methodology, Investigation, Formal analysis, Data curation, Conceptualization. **J.H.S. Martins:** Conceptualization, Methodology, Investigation, Writing – review & editing. **D. Dimitrakis:** Writing – review & editing, Supervision, Resources, Project administration, Methodology, Investigation, Funding acquisition, Conceptualization. **D. Thomey:** Writing – review & editing, Project administration, Funding acquisition, Supervision. **N. Monnerie:** Writing – review & editing, Supervision. **C. Sattler:** Writing – review & editing, Supervision. **J. Michels:** Writing – review & editing, Resources, Methodology, Investigation. **M. Kürten:** Writing – review & editing. **M. Lanchi:** Writing – review & editing. **R. Liberatore:** Writing – review & editing. **L. Turchetti:** Writing – review & editing.

Declaration of competing interest

The authors declare that they have no known competing financial interests or personal relationships that could have appeared to influence the work reported in this paper.

Acknowledgments

The authors thank the European Commission for co-funding the EU Horizon project HySelect under the Grant Agreement No. 101101498, supported by the Clean Hydrogen Partnership and its members Hydrogen Europe and Hydrogen Europe Research.

Appendix A. Supplementary files

Supplementary files to this article can be found online at https://doi.org/10.1016/j.seta.2026.105361.

Data availability

Data will be made available on request.

References

[1] Farbman GH. Hydrogen production by the Westinghouse sulfur cycle process: program status. Int J Hydrog Energy 1979;4:111–22. https://doi.org/10.1016/0360-3199(79)90045-4.
[2] Muller TL. Sulfuric acid and sulfur trioxide. Kirk-Othmer Encyclopedia of Chemical Technology. 2006. Doi: 10.1002/0471238961.1921120613211212.a01.pub2.
[3] Díaz-Abad S, Millán M, Rodrigo MA, et al. Review of anodic catalysts for SO2 depolarized electrolysis for "green hydrogen". Product Catal 2019;9:63. https://doi.org/10.3390/catal9010063.
[4] Chen C, Jiao F, Lu B, et al. Thermochemical water splitting cycles for hydrogen production: Perspectives for thermodynamic approaches. Appl Energy 2025;377:124599. https://doi.org/10.1016/j.apenergy.2024.124599.
[5] Yılmaz F, Balta MT. Energy and exergy analyses of hydrogen production step in boron based thermochemical cycle for hydrogen production. Int J Hydrog Energy 2017;42:2485–91. https://doi.org/10.1016/j.ijhydene.2016.04.017.
[6] Safari F, Dincer I. A review and comparative evaluation of thermochemical water splitting cycles for hydrogen production. Energy Convers Manag 2020;205:112182. https://doi.org/10.1016/j.enconman.2019.112182.

[7] Xie L, Zhang P, Tian R, et al. Research progress in SO2 depolarized electrolysis at INET. Renew Energy 2025;242:122424. https://doi.org/10.1016/j.renene.2025.122424.
[8] Haussener S. Solar fuel processing: comparative mini-review on research, technology development, and scaling. Sol Energy 2022;246:294–300. https://doi.org/10.1016/j.solener.2022.09.019.
[9] McGregor C, Singh VP, Kumar A. The pivotal role of high-temperature solar thermal energy in a sustainable future. In: McGregor C, Singh VP, Kumar A, editors. High-Temperature Solar Thermal Systems: Volume 1—Fundamentals, Innovations, and Advances. Cham: Springer Nature Switzerland; 2025. p. 1–28. 10.1007/978-3-032-07641-0_1.
[10] Singh VP, McGregor C. Generation classification of solar thermal technologies. Renew Sustain Energy Rev 2026;230:116705. https://doi.org/10.1016/j.rser.2026.116705.
[11] Lubkoll M, Ebert M, Amsbeck L, et al. Development progress of the CentRec® particle receiver technology. AIP Conf Proc 2022;2445:110005. https://doi.org/10.1063/5.0086510.
[12] Zavattoni SA, Montorfano D, Good P, et al. Synhelion absorbing gas solar receiver – Design advancement. AIP Conf Proc 2023;2815:100016. https://doi.org/10.1063/5.0149049.
[13] Gorensek MB. Hybrid sulfur cycle flowsheets for hydrogen production using high-temperature gas-cooled reactors. Int J Hydrog Energy 2011;36:12725–41. https://doi.org/10.1016/j.ijhydene.2011.07.033.
[14] Gorensek MB, Summers WA. Hybrid sulfur flowsheets using PEM electrolysis and a bayonet decomposition reactor. Int J Hydrog Energy 2009;34:4097–114. https://doi.org/10.1016/j.ijhydene.2008.06.049.
[15] Guerra Niehoff A, Bayer Botero N, Acharya A, et al. Process modelling and heat management of the solar hybrid sulfur cycle. Int J Hydrog Energy 2015;40:4461–73. https://doi.org/10.1016/j.ijhydene.2015.01.168.
[16] Gorensek MB, Corgnale C, Summers WA. Development of the hybrid sulfur cycle for use with concentrated solar heat. I. Conceptual design. Int J Hydrog Energy 2017;42:20939–54. https://doi.org/10.1016/j.ijhydene.2017.06.241.
[17] Uygun Batgi S, Dincer I. A solar driven hybrid sulfur cycle based integrated hydrogen production system for useful outputs. Int J Hydrog Energy 2023;48:34316–29. https://doi.org/10.1016/j.ijhydene.2023.05.199.
[18] Corgnale C, Summers WA. Solar hydrogen production by the Hybrid Sulfur process. Int J Hydrog Energy 2011;36:11604–19. https://doi.org/10.1016/j.ijhydene.2011.05.173.
[19] Del Fabbro Arcopinto GL. Techno economic analysis of the Hybrid sulfur cycle for the production of hydrogen through solar source. Rome: Università Campus Bio-Medico; 2021. Master's thesis.
[20] Zuleta Marin JS, Bern G, Platzer W, et al. Implementation of a solar-assisted hybrid sulfur cycle for hydrogen and oxygen production in the Chilean copper industry. Sol Energy 2026;311:114530. https://doi.org/10.1016/j.solener.2026.114530.
[21] Commissariat à l'énergie atomique et aux énergies alternatives (2011) Final Report Summary - HYTHEC (High Temperature Thermochemical Cycles). https://cordis.europa.eu/project/id/502704/reporting. Accessed 01 Aug 2026.
[22] Le Duigou A, Borgard J-M, Larousse B, et al. HYTHEC: an EC funded search for a long term massive hydrogen production route using solar and nuclear technologies. Int J Hydrog Energy 2007;32:1516–29. https://doi.org/10.1016/j.ijhydene.2006.10.047.
[23] Noglik A, Roeb M, Sattler C, et al. Numerical optimization of a volumetric solar receiver-reactor for thermochemical hydrogen generation via decomposition of sulfur trioxide. In: Proceedings of ASME 4th International Conference on Energy Sustainability, Phoenix, Arizona, USA; 2010. p. 183–92. https://doi.org/10.1115/es2010-90125.
[24] Noglik A, Roeb M, Sattler C, et al. Experimental study on sulfur trioxide decomposition in a volumetric solar receiver–reactor. Int J Energy Res 2009;33:799–812. https://doi.org/10.1002/er.1514.
[25] Monnerie N, Schmitz M, Roeb M, et al. Potential of hybridisation of the thermochemical hybrid-sulphur cycle for the production of hydrogen by using nuclear and solar energy in the same plant. Int J Nucl Hydrogen Prod Appl 2011;2:178–201. https://doi.org/10.1504/IJNHPA.2011.038343.
[26] Roeb M (2013) Final Report Summary - HYCYCLES (Materials and components for hydrogen production by sulphur based thermochemical cycles). https://cordis.europa.eu/project/id/212470/reporting. Accessed 27 Jan 2026.
[27] Haussener S, Thomey D, Roeb M, et al. Multi-scale modelling of a solar reactor for the high-temperature step of a sulphur-iodine-based water splitting cycle. In: Grande R, Rico P, editors. In: Proceedings of ASME 2012 Summer Heat Transfer Conference; 2012. p. 287–96. https://doi.org/10.1115/HT2012-58323.
[28] Thomey D, de Oliveira L, Säck J-P, et al. Development and test of a solar reactor for decomposition of sulphuric acid in thermochemical hydrogen production. Int J Hydrog Energy 2012;37:16615–22. https://doi.org/10.1016/j.ijhydene.2012.02.136.
[29] Karagiannakis G, Agrafiotis CC, Zygogianni A, et al. Hydrogen production via sulfur-based thermochemical cycles: Part 1: Synthesis and evaluation of metal oxide-based candidate catalyst powders for the sulfuric acid decomposition step. Int J Hydrog Energy 2011;36:2831–44. https://doi.org/10.1016/j.ijhydene.2010.11.083.
[30] Giaconia A, Sau S, Felici C, et al. Hydrogen production via sulfur-based thermochemical cycles: Part 2: Performance evaluation of Fe2O3-based catalysts for the sulfuric acid decomposition step. Int J Hydrog Energy 2011;36:6496–509. https://doi.org/10.1016/j.ijhydene.2011.02.137.
[31] Karagiannakis G, Agrafiotis CC, Pagkoura C, et al. Hydrogen production via sulfur-based thermochemical cycles: Part 3: Durability and post-characterization of silicon carbide honeycomb substrates coated with metal oxide-based candidate catalysts for the sulfuric acid decomposition step. Int J Hydrog Energy 2012;37:8190–203. https://doi.org/10.1016/j.ijhydene.2012.02.090.
[32] Odorizzi S, Baldasso C, Gasik M (2017) Final Report Summary - SOL2HY2 (Solar To Hydrogen Hybrid Cycles). https://cordis.europa.eu/project/id/325320/reporting. Accessed 24 Feb 2025.
[33] Bayer Botero N, Thomey D, Guerra Niehoff A, et al. Modelling and scaling analysis of a solar reactor for sulphuric acid cracking in a hybrid sulphur cycle process for thermochemical hydrogen production. Int J Hydrog Energy 2016;41:8008–19. https://doi.org/10.1016/j.ijhydene.2015.11.088.
[34] Lapp JL, Guerra-Niehoff A, Streber H-P, et al. Modeling of a solar receiver for superheating sulfuric acid. J Sol Energy Eng 2016;138:41013. https://doi.org/10.1115/1.4033594.
[35] Santasalo-Aarnio A, Virtanen J, Gasik M. SO2 carry-over and sulphur formation in a SO2-depolarized electrolyser. J Solid State Electrochem 2016;20:1655–63. https://doi.org/10.1007/s10008-016-3169-8.
[36] Santasalo-Aarnio A, Lokkiluoto A, Virtanen J, et al. Performance of electrocatalytic gold coating on bipolar plates for SO2 depolarized electrolyser. J Power Sources 2016;306:1–7. https://doi.org/10.1016/j.jpowsour.2015.11.104.
[37] Gasik MM, Virtanen J, Santasalo-Aarnio A. Improved operation of SO2 depolarized electrolyser stack for H2 production at ambient conditions. Int J Hydrog Energy 2017;42:13407–14. https://doi.org/10.1016/j.ijhydene.2017.03.003.
[38] Liberatore R, Bassi A, Turchetti L, et al. Multi-objective optimization of a hydrogen production through the HyS process powered by solar energy in different scenarios. Int J Hydrog Energy 2018;43:8683–97. https://doi.org/10.1016/j.ijhydene.2018.03.109.
[39] DLR - Institute of Solar Research (2016) Pegasus Project: Home. https://www.pegasus-project.eu/. Accessed 17 Feb 2025.
[40] Chen S, Zhang P, Wang L, et al. Development of a prototype of helium-heated sulfuric acid decomposer for sulfur-family thermochemical water splitting process. Int J Hydrog Energy 2025;180:151782. https://doi.org/10.1016/j.ijhydene.2025.151782.
[41] Zeng J, Song W, Zhang K, et al. Material selection, simulation, and experimentation of sulfuric acid decomposition in a pilot-scale sulfur-iodine thermochemical cycle for hydrogen production. Fuel 2026;426:139556. https://doi.org/10.1016/j.fuel.2026.139556.
[42] FEN Research GmbH (2024) HySelect. https://hyselect.eu/. Accessed 04 Jul 2026.
[43] Lanchi M, Liberatore R, Battaglia M, et al. Flexible green hydrogen production through the HyS cycle: process analysis of different concepts for the HySelect demo plant. Int J Hydrog Energy 2025;127:64–84. https://doi.org/10.1016/j.ijhydene.2025.04.095.
[44] Imran Khan M, Asfand F, Al-Ghamdi SG. Progress in research and technological advancements of commercial concentrated solar thermal power plants. Sol Energy 2023;249:183–226. https://doi.org/10.1016/j.solener.2022.10.041.
[45] Mordor Intelligence (2026) Sulfuric Acid Market Size and Share Analysis - Growth Trends and Forecast (2026 - 2031). https://www.mordorintelligence.com/industry-reports/sulfuric-acid-market. Accessed 30 Jan 2026.
[46] Elouaer Y, Mabrouk A, Gonzalez-Alriols M, et al. Innovative approach to SO_2 control in sulphuric acid plants using oxygen-enriched air. Process Integr. Optim. Sustain 2026. https://doi.org/10.1007/s41660-026-00810-0.
[47] U.S. Environmental Protection Agency (2023) Response to Comments on the 2022 Proposed Rule: Accidental Release Prevention Requirements: Risk Management Programs Under the Clean Air Act; Safer Communities by Chemical Accident Prevention.
[48] Melnikova N, Wu J, Ruiz P, et al. National toxic substances incidents program — Nine States, 2010–2014. MMWR Surveill Summaries 2020;69:1–10. https://doi.org/10.15585/mmwr.ss6902a1.
[49] King M, Fenton M, Huebsch J, et al. The Forgotten Heart of the Phosphate Fertilizer Complex. World Fertilizer 2025:20–3. ISSN: 2398-4384.
[50] Occupational Safety and Health Administration. OSHA Accident Report Detail: Release of Sulfur Dioxide and Trioxide at a Facility. Accessed 10 Aug 2026, https://www.osha.gov/ords/imis/accidentsearch.accident_detail%3Fid%3D201484300; 2001.
[51] Kawazoe M, Tomoda Y, Sasaki A et al. (1979) Method of controlling the suction gas pressure of a sulfuric acid plant for treatment of smelter exhaust gas. (US4281821A). https://patents.google.com/patent/US4281821A/en. Accessed 10 Aug 2026.
[52] Badini C, de Haan F, Celasco E, et al. Corrosion Behavior of SiC Laminate under Decomposed Sulfuric Acid at 850°C. J Am Ceram Soc 2012;95:2627–34. https://doi.org/10.1111/j.1551-2916.2012.05337.x.
[53] Agrafiotis C, Thomey D, de Oliveira L, et al. Structured sulphur trioxide splitting catalytic systems and allothermally-heated reactors for the implementation of Sulphur-based thermochemical cycles via a centrifugal solar particle receiver. Appl Catal, B 2023;324:122197. https://doi.org/10.1016/j.apcatb.2022.122197.
[54] Zeng J, He Y, Zhang J, et al. Design monolithic honeycomb SiC catalysts via industrial-grade DLP 3D printing technology for practical sulfur-based thermochemical hydrogen production. Int J Hydrog Energy 2026;207:153462. https://doi.org/10.1016/j.ijhydene.2026.153462.
[55] Clean Hydrogen Joint Undertaking (2022) Clean Hydrogen JU - SRIA Key Performance Indicators (KPIs). https://www.clean-hydrogen.europa.eu/knowledge-management/strategy-map-and-key-performance-indicators/clean-hydrogen-ju-sria-key-performance-indicators-kpis_en. Accessed 09 Sep 2025.
[56] Buck R, Sment J. Techno-economic analysis of multi-tower solar particle power plants. Sol Energy 2023;254:112–22. https://doi.org/10.1016/j.solener.2023.02.045.

[57] TECHO (2026) How Centrifugal Pumps Work: Comprehensive Guide 2026. https://www.cntecho.com/centrifugal-pump-guide-principles-selection-maintenance-2026. Accessed 27 Apr 2026.
[58] Bloch HP. Reciprocating compressor performance and sizing fundamentals. In: A Practical Guide to Compressor Technology. John Wiley & Sons Inc; 2006. p. 171–96. https://doi.org/10.1002/0471929786.
[59] Folkers S, Welp A, Heselmann M, et al. Fluid mixtures in three compressor types for charging carnot-batteries: efficiencies and combined fluid-machine selection. In: Proceedings of 38th International Conference on Efficiency, Cost, Optimization, Simulation and Environmental Impact of Energy Systems (ECOS 2025), Paris, France; 2025. p. 1–12. Doi: 10.17185/duepublico/84666.
[60] True Geometry's Blog (2024) Understanding Hoist Motor Efficiency and Its Impact on Power Consumption in context of hoist motor power. https://blog.truegeometry.com/tutorials/education/b6d5fae7ae78d5c673dee2a8ddae6e40/JSON_TO_ARTCL_Understanding_Hoist_Motor_Efficiency_and_Its_Impact_on_Power_Consu.html. Accessed 27 Apr 2026.
[61] Phelps EH, Vreeland DC. Corrosion of Austenitic Stainless Steels in Sulfuric Acid. Corrosion 1957;13:21–6. https://doi.org/10.5006/0010-9312-13.10.21.
[62] Data Bridge Market Research (2025) Global Sulfuric Acid Market Size, Share, and Trends Analysis Report - Industry Overview and Forecast to 2032. https://www.databridgemarketresearch.com/reports/sulfuric-acid-market. Accessed 23 Jan 2026.
[63] Cerqueira EP, Novais WRI, Narváez-Romo B, et al. A comparative analysis between absorption and vapor compression refrigeration systems. In: COBEM 2021: 26th International Congress of Mechanical Engineering, São Paulo, Brazil; 2021. https://doi.org/10.26678/ABCM.COBEM2021.COB2021-0990.
[64] Que H, Song Y, Chen C-C. Thermodynamic modeling of the sulfuric acid−water−sulfur trioxide system with the symmetric electrolyte NRTL model. J Chem Eng Data 2011;56:963–77. https://doi.org/10.1021/je100930y.
[65] Corgnale C, Gorensek MB, Summers WA. Review of sulfuric acid decomposition processes for sulfur-based thermochemical hydrogen production cycles. Processes 2020;8:1383. https://doi.org/10.3390/pr8111383.
[66] Albrecht FG, König DH, Baucks N, et al. A standardized methodology for the techno-economic evaluation of alternative fuels – a case study. Fuel 2017;194:511–26. https://doi.org/10.1016/j.fuel.2016.12.003.
[67] Townsend W, Faber G (2021) AssessCCUS Capital Equipment Cost Database. https://assessccus.globalco2initiative.org/wp-content/uploads/Capital-Equipment-Cost-Database.xlsx. Accessed 23 Jan 2026.
[68] Woods DR. Rules of Thumb in Engineering Practice. 1st ed. Weinheim, Germany: Wiley-VCH Verlag GmbH & Co. KGaA; 2007. 10.1002/9783527611119.
[69] Sinnott R, Towler G. Chapter 6 - costing and project evaluation. In: Chemical engineering design (sixth edition): chemical engineering series. Butterworth-Heinemann; 2020. p. 275–369. Doi: 10.1016/B978-0-08-102599-4.00006-0.
[70] Charles Maxwell (2026) Cost Indices. https://toweringskills.com/financial-analysis/cost-indices/. Accessed 04 Aug 2026.
[71] Ullrich H. Wirtschaftliche Planung und Abwicklung verfahrenstechnischer Anlagen (HDT-Fachbuchreihe). Vulkan-Verlag GmbH 1996. ISBN: 978-3-8027-8515-3.
[72] Statistisches Bundesamt (2026) Earnings by economic activity April 2024: Earnings and earnings differences. https://www.destatis.de/EN/Themes/Labour/Earnings/Branch-Occupation/Tables/quaterly-earnings.html. Accessed 09 Feb 2026.
[73] Schemme S. Techno-ökonomische Bewertung von Verfahren zur Herstellung von Kraftstoffen aus H2 und CO2. Aachen: RWTH Aachen University; 2020. ISBN: 978-3-95806-499-7. PhD thesis.
[74] European Parliament and Council (1996) Directive 96/53/EC of 25 July 1996 laying down for certain road vehicles circulating within the Community the maximum authorised dimensions and weights. https://eur-lex.europa.eu/legal-content/EN/TXT/?uri=CELEX%3A31996L0053. Accessed 27 Jan 2026.
[75] Bundesnetzagentur (2025) Industrial electricity prices: Modelled industrial electricity prices since 2020. https://www.smard.de/page/en/topic-article/5790/216084/industrial-electricity-prices. Accessed 27 Jan 2026.
[76] Lackovic L, Buck R (2024) Development of centrifugal particle receivers. https://www.energy.gov/sites/default/files/2024-02/3.2%20240215_Pres_DLR_ParticleTechnology.pdf. Accessed 23 Jan 2026.
[77] Buck R, Giuliano S. Impact of solar tower design parameters on sCO2-based solar tower plants. In: Proceedings of 2nd European sCO2 Conference 2018. Essen, Germany: University Duisburg-Essen; 2018. https://doi.org/10.17185/duepublico/46098.
[78] Verma M, Singh VP. Techno-economic assessment of high-temperature solar thermal systems. In: McGregor C, Singh VP, Kumar A, editors. High-Temperature Solar Thermal Systems: Volume 1—Fundamentals, Innovations, and Advances. Cham: Springer Nature Switzerland; 2025. p. 407–30.
[79] Santini M, Dwyer T. Module 91: High-efficiency waste heat-powered lithium bromide absorption chillers. CIBSE J 2016. https://www.cibsejournal.com/cpd/modules/2016-03-chil/.
[80] NH3 Solutions Standard and customised ammonia chillers and heat pumps. https://nh3solutions.com/en/ammonia-chillers-and-heat-pumps/. Accessed 12 Aug 2026.
[81] Yao Y, Hu Y, Gao S. Heliostat field layout methodology in central receiver systems based on efficiency-related distribution. Sol Energy 2015;117:114–24. https://doi.org/10.1016/j.solener.2015.04.029.
[82] Corsi C, Blanco MJ, Grigoriev V, et al. Upper limits to the mean annual optical efficiency of solar mono-tower systems. Sol Energy 2022;236:88–99. https://doi.org/10.1016/j.solener.2022.02.038.
[83] Paul I, Kedare SB. Mirror density optimization of solar tower system considering optical and receiver parameters. Sol Energy 2026;308:114375. https://doi.org/10.1016/j.solener.2026.114375.
[84] Liberatore R, Lanchi M, Giaconia A, et al. Energy and economic assessment of an industrial plant for the hydrogen production by water-splitting through the sulfur-iodine thermochemical cycle powered by concentrated solar energy. Int J Hydrog Energy 2012;37:9550–65. https://doi.org/10.1016/j.ijhydene.2012.03.088.
[85] Boretti A. Technology readiness level of solar thermochemical splitting cycles. ACS Energy Lett 2021;6:1170–4. https://doi.org/10.1021/acsenergylett.1c00181.
[86] International Energy Agency (2026) ETP Clean Energy Technology Guide. https://www.iea.org/data-and-statistics/data-tools/etp-clean-energy-technology-guide. Accessed 13 Aug 2026.
[87] Yilmaz F, Selbaş R. Thermodynamic performance assessment of solar based Sulfur-Iodine thermochemical cycle for hydrogen generation. Energy 2017;140:520–9. https://doi.org/10.1016/j.energy.2017.08.121.
[88] Zeng J, He Y, Song W, et al. Concentrated solar-powered sulfur-iodine thermochemical cycle hydrogen production system: Energy, economic, and environmental assessment. Energy Convers Manag 2026;356:121345. https://doi.org/10.1016/j.enconman.2026.121345.
[89] Temiz M, Dincer I. Concentrated solar driven thermochemical hydrogen production plant with thermal energy storage and geothermal systems. Energy 2021;219:119554. https://doi.org/10.1016/j.energy.2020.119554.
[90] Khormi NA, Fronk BM. Techno-economic comparison of particle and gas-based central solar thermal receiver systems for the cogeneration of electricity and hydrogen. J Sol Energy Eng 2025;147:51009. https://doi.org/10.1115/1.4068813.
[91] Sharma JP, Kumar R, Ahmadi MH, et al. Thermodynamic analysis on CSP integrated cerium oxide (CeO2 − CeO1.72/1.83) water splitting cycle for hydrogen production. Int J Hydrog Energy 2024;53:1259–68. https://doi.org/10.1016/j.ijhydene.2023.11.338.
[92] Lou J, Lu X, Wu Y, et al. Thermodynamic evaluation of nonstoichiometric oxides for efficient and practical solar thermochemical hydrogen production. Energy Convers Manag 2024;314:118156. https://doi.org/10.1016/j.enconman.2024.118156.
[93] Mastropasqua L, Pecenati I, Giostri A, et al. Solar hydrogen production: Techno-economic analysis of a parabolic dish-supported high-temperature electrolysis system. Appl Energy 2020;261:114392. https://doi.org/10.1016/j.apenergy.2019.114392.
[94] Hassan A, Yousuf S, Deng Z, et al. Solar-driven green hydrogen production: Comparative pathways, technical challenges, and future perspectives. Int J Hydrog Energy 2025;195:152516. https://doi.org/10.1016/j.ijhydene.2025.152516.
[95] Yadav D, Banerjee R. Economic assessment of hydrogen production from solar driven high-temperature steam electrolysis process. J Clean Prod 2018;183:1131–55. https://doi.org/10.1016/j.jclepro.2018.01.074.
[96] Calnan S, Bagacki R, Bao F, et al. Development of various photovoltaic-driven water electrolysis technologies for green solar hydrogen generation. Sol RRL 2022;6:2100479. https://doi.org/10.1002/solr.202100479.
[97] Arunachalam M, Han DS. Efficient solar-powered PEM electrolysis for sustainable hydrogen production: an integrated approach. Emergent Mater 2024;7:1401–15. https://doi.org/10.1007/s42247-024-00697-y.
[98] Niederhofer S, Rennhofer M, Hofmann R, et al. System efficiency analysis of direct coupled PV–PEM electrolyzer systems. Int J Hydrog Energy 2025;185:151860. https://doi.org/10.1016/j.ijhydene.2025.151860.